

# Phosphorus-Based Composites as Anode Materials for Advanced Alkali Metal Ion Batteries

Junhua Zhou, Qitao Shi, Sami Ullah, Xiaoqin Yang, Alicja Bachmatiuk, Ruizhi Yang,\* and Mark H. Rummeli\*

Alkaline metal ion batteries, such as lithium-ion batteries have been increasingly adopted in consumer electronics, electric vehicles, and large power grids because of their high energy density, power density and working voltage, and long cycle life. Phosphorus-based materials including phosphorus anodes and metal phosphides with high theoretical capacity, natural abundance, and environmental friendliness show great potential as negative electrodes for alkaline metal ion batteries. In this review, based on the understanding of the storage mechanism of alkali metal ions, the scientific challenges are discussed, the preparation methods and solutions to address these challenges are summarized, the application prospects are demonstrated, and finally possible future research directions of phosphorus-based materials are provided.

sodium and potassium belong to the same group with lithium in the periodic table. Therefore, AIBs have the similar chemical properties, and SIBs and PIBs may adopt alike electrode materials, electrolyte, and battery manufacturing process developed for LIBs.<sup>[6,7]</sup>

Energy density is one of the most critical parameters for battery system, and it can be roughly calculated by the following formula

$$E_m = \frac{Q_c \times Q_a}{Q_c + Q_a} \times (U_c - U_a) \times K \quad (1)$$


in which  $E_m$ ,  $Q_c$ ,  $Q_a$ ,  $U_c$ ,  $U_a$ , and  $K$  are the energy density, specific capacity of cathode and anode, average potential of cathode and anode, and the proportion of active materials in battery, respectively.<sup>[8]</sup> In LIBs, the  $K$  value is usually between 0.42 and 0.61. It can be seen from the above formula that strategies to improve energy density mainly include enhancing the specific capacity of cathode or anode, using higher potential material for cathode or lower one for anode, and increasing the  $K$  value. (The  $K$  value is mainly related to the battery manufacturing process, which is not in the scope of this paper.)

Tuning the capacity and voltage of electrode materials is the main strategy to improve the energy density of battery.<sup>[9]</sup> A common approach is finding negative electrode materials with high specific capacity and low potential. Alloy-based materials such as Si, Ge, Sn, P, Sb, Bi, Se, and Zn can react with Li, Na, and K based on multi-electron transfer.<sup>[7,10]</sup> They have high

## 1. Introduction

With the aggravation of energy and environmental crises, rechargeable battery like lithium ion batteries (LIBs) have wide application prospects in portable consumer electronics, electric vehicles, and energy storage grids.<sup>[1–4]</sup> In addition to LIBs, sodium ion batteries (SIBs) and potassium ion batteries (PIBs) have attracted extensive attention recently due to their abundant resources.<sup>[5]</sup> These alkaline metal ion batteries (AIBs) have several advantages compared with other battery systems such as aluminum ion batteries and magnesium ion batteries. First, AIBs show relatively low electrochemical potential owing to the strong electronegativity of alkali metal ions ( $A^+$ ), resulting in high energy density. Second, the weaker Coulombic interaction between monovalent ions ( $A^+$ ) accelerates kinetics. Third,

J. H. Zhou, Q. T. Shi, S. Ullah, X. Q. Yang, Prof. A. Bachmatiuk, Prof. R. Z. Yang, Prof. M. H. Rummeli  
 College of Energy  
 Soochow Institute for Energy and Materials InnovationS (SIEMIS)  
 Key Laboratory of Advanced Carbon Materials and Wearable Energy  
 Technologies of Jiangsu Province  
 Soochow University  
 Suzhou 215006, China  
 E-mail: yangrz@suda.edu.cn; mhr1@suda.edu.cn

 The ORCID identification number(s) for the author(s) of this article can be found under <https://doi.org/10.1002/adfm.202004648>.

© 2020 The Authors. Published by Wiley-VCH GmbH. This is an open access article under the terms of the Creative Commons Attribution License, which permits use, distribution and reproduction in any medium, provided the original work is properly cited.

DOI: 10.1002/adfm.202004648

X. Q. Yang  
 School of Energy and Power Engineering  
 Xi'an Jiaotong University  
 No. 28, Xianning West Road, Xi'an, Shaanxi 710049, China  
 Prof. A. Bachmatiuk  
 LUKASIEWICZ Research Network  
 PORT Polish Center for Technology Development  
 Stablowicka 147, Wroclaw 54-066, Poland  
 Prof. M. H. Rummeli  
 Leibniz Institute for Solid State and Materials Research Dresden  
 P.O. Box 270116 D-01171, Dresden, Germany  
 Prof. M. H. Rummeli  
 Centre of Polymer and Carbon Materials  
 Polish Academy of Sciences  
 M. Curie-Sklodowskiej 34, Zabrze 41-819, Poland  
 Prof. M. H. Rummeli  
 Institute of Environmental Technology  
 VSB-Technical University of Ostrava  
 17. Listopadu 15, Ostrava 708 33, Czech Republic

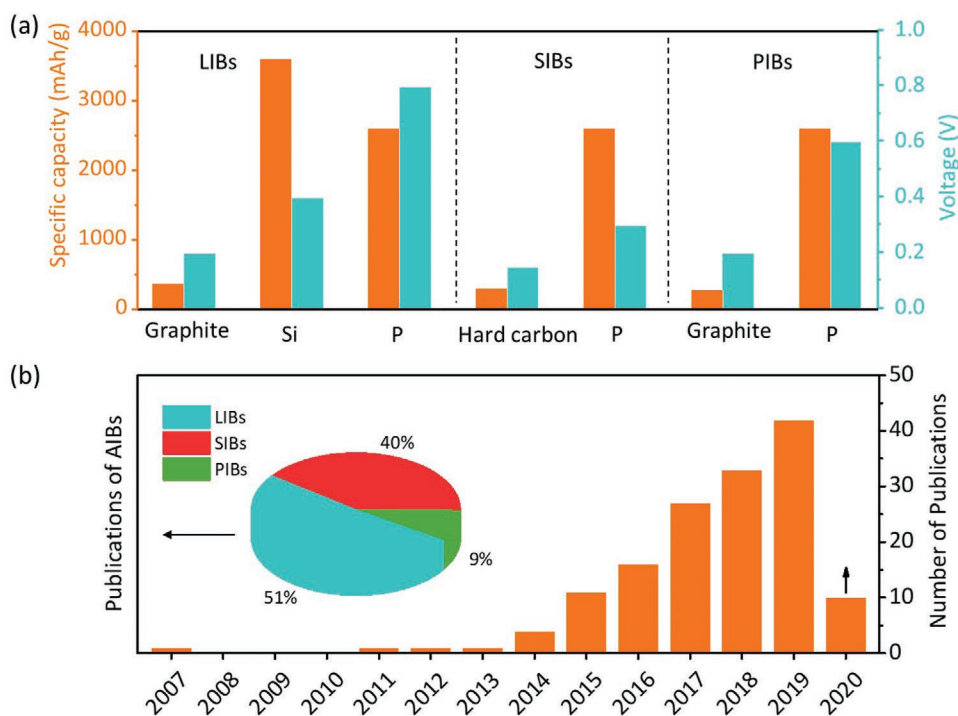


**Figure 1.** Advantages of phosphorus anodes for AIBs: a) Theoretical specific capacity and average working voltage of typical anodes in LIBs, SIBs, and PIBs; b) Number of publications on phosphorus-based anodes according to the Web of Science (as of Apr. 2020).

theoretical specific capacity and low electrode potential, and hence are ideal anode materials for AIBs. For LIBs, although silicon anodes exhibit extremely large theoretical specific capacity ( $4200 \text{ mA h g}^{-1}$ ), the practical value is generally only  $400\text{--}600 \text{ mA h g}^{-1}$  because compounding with graphite is necessary to limit the huge volume expansion of Si during charging and discharging process.<sup>[11]</sup> While the average potential of phosphorus in LIBs is comparatively high ( $\approx 0.8 \text{ V vs Li/Li}^+$ ), its large specific capacity ( $2590 \text{ mA h g}^{-1}$ ) may compensate for this flaw (Figure 1a). For SIBs, phosphorus exhibits the highest theoretical specific capacity ( $2590 \text{ mA h g}^{-1}$ ) among all anode materials and considerably low work potential ( $\approx 0.3 \text{ V vs Na/Na}^+$ ), making its superiority obvious.<sup>[12–14]</sup> For PIBs, its theoretical specific capacity is also the largest (the value may be  $2590 \text{ mA h g}^{-1}$  based on  $\text{K}_3\text{P}$ ) and the average voltage is moderate ( $\approx 0.6 \text{ V vs K/K}^+$ ).<sup>[15]</sup> In addition, phosphorus can be derived from rich resources, has low price, and exhibits minor pollution potential.<sup>[16–18]</sup> Thus, phosphorus-based anode materials show great potential in AIBs and have recently attracted extensive attention from researchers (Figure 1b). Because of the partial similarity between phosphorus anode (P anode) and metal phosphides ( $\text{M}_x\text{P}_y$ ) systems, in this review we consider both as phosphorus-based composites.

## 2. Alkaline Metal Ions Storage Mechanism

### 2.1. P Anode

The mechanism for  $\text{A}^+$  ion storage in electrode materials determines its electrochemical performance in AIBs, and this is usually studied by advanced ex situ or in situ technologies

such as XRD, XAS, TEM, solid-state NMR, and Raman.<sup>[19,20]</sup> There are three main allotropes of phosphorus in nature, namely white phosphorus (WP), red phosphorus (RP), and black phosphorus (BP) (Figure 2a). Among them, WP is highly toxic and easily self-ignites in air, and thus it is not suitable for electrode material. RP exhibits amorphous structure and very low conductivity ( $10^{-14} \text{ S cm}^{-1}$ ), while BP shows graphite-like layered structure and better conductivity ( $0.2\text{--}3.3 \text{ S cm}^{-1}$ ).<sup>[21]</sup> Considering the huge difference in price between RP ( $\approx 0.261 \text{ RMB g}^{-1}$ ) and BP ( $\approx 3240 \text{ RMB g}^{-1}$ ), RP is usually used as raw materials for the synthesis of BP, phosphorus/carbon composites (P/C), and  $\text{M}_x\text{P}_y$ .

The various allotropes exhibit diverse charge and discharge mechanisms. Ex situ XRD investigations showed that RP went through alloying reaction. The insertion of  $\text{Li}^+$  in amorphous RP first forms amorphous Li–P alloys, finally transformed into crystalline  $\text{Li}_3\text{P}$  (c- $\text{Li}_3\text{P}$ ), and the charge process was basically reversible (Figure 2b).<sup>[22]</sup> However, XRD is mainly sensitive to crystalline materials, and the amorphous products should be further characterized by NMR. Ex situ solid-state NMR spectra displayed that the lithiation process was  $\text{RP} \rightarrow (\text{LiP}_7, \text{LiP}_5, \text{Li}_3\text{P}_7, \text{LiP}) \rightarrow \alpha\text{-Li}_3\text{P} \rightarrow \text{c-Li}_3\text{P} \rightarrow \text{Li}_{3+x}\text{P}$  and the delithiation process was  $\text{Li}_{3+x}\text{P} \rightarrow \text{c-Li}_3\text{P} \rightarrow (\text{Li}_3\text{P}_7, \text{LiP}_5, \text{LiP}_7) \rightarrow \text{RP}$  (Figure 2c). Irreversible capacity loss occurred because of the incomplete symmetry between the charge and discharge processes and the formation of inactive phases such as  $\text{Li}_3\text{PO}_4$ .

BP displays the 2D layered structure, which can be converted into phosphorene with only a few atomic layers by physical or chemical stripping methods (will be discussed in Section 4.1). Sun et al. prepared graphene–phosphorene composites by liquid phase exfoliation (LPE), and explored the sodiation mechanism with the first step of  $\text{Na}^+$  intercalation, and

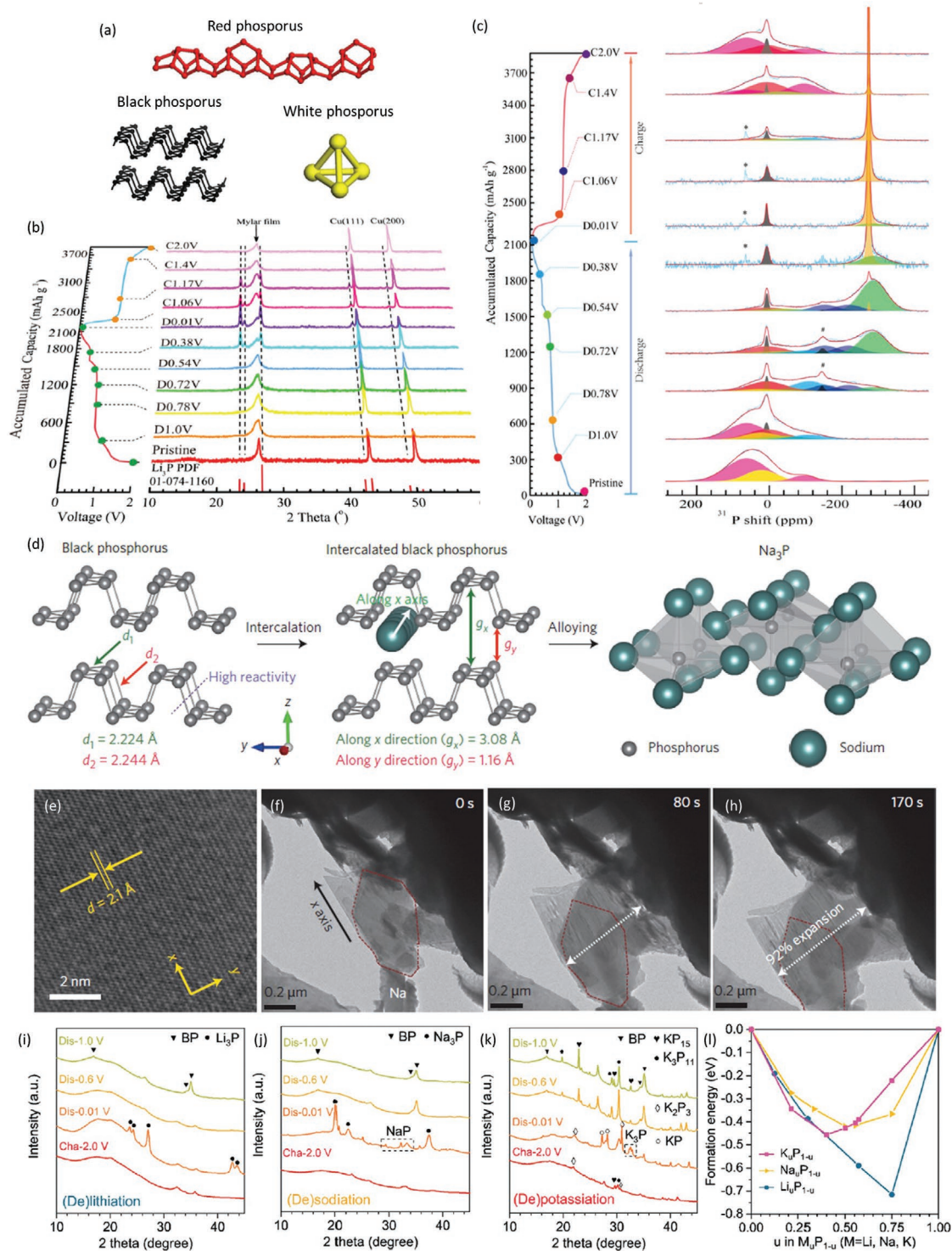


**Figure 2.** Alkaline metal ions storage mechanisms of P anode in AIBs: a) Schematics of WP, RP, and BP; b) Ex situ XRD patterns of RP/C at various potential; c) Ex situ <sup>31</sup>P spectra of RP/C; d) Mechanism of BP in SIBs, with the first step of intercalation and the second step of alloy reaction; e–h) In situ TEM images of BP in SIBs; i–k) Ex situ XRD patterns of BP-graphite electrodes in LIBs, SIBs, and PIBs; l) Formation energy in M-P (M = Li, Na, and K) compounds. a) Reproduced with permission.<sup>[21]</sup> Copyright 2014, American Chemical Society. b,c) Reproduced with permission.<sup>[22]</sup> Copyright 2019, Elsevier. d–h) Reproduced with permission.<sup>[23]</sup> Copyright 2015, Macmillan Publishers Limited. i–l) Reproduced with permission.<sup>[24]</sup> Copyright 2019, Wiley-VCH.

the second step of alloy reaction to form  $\text{Na}_3\text{P}$  (Figure 2d).<sup>[23]</sup> In ex situ XRD spectra, when the discharge voltage was above 0.54 V (vs  $\text{Na}/\text{Na}^+$ ), the position of diffraction peaks did not change, suggesting an intercalation mechanism. After the discharge voltage was lower than 0.54 V (vs  $\text{Na}/\text{Na}^+$ ), first the diffraction peaks disappeared completely and thus indicated the formation of amorphous intermediate products, and finally weak diffraction peaks emerged due to the formation of crystallized  $\text{Na}_3\text{P}$ . The in situ TEM images demonstrated anisotropic volume change of phosphorene: there was basically no change in the X direction, the Y direction expanded by 92%, and the Z direction swelled by 160%, mainly because sodium ions preferentially diffused along the X direction (Figure 2e–h).

Phosphorus can be acted as anode universally in AIBs, and the difference of their specific capacity is huge. Jin et al. revealed the distinct charge and discharge behavior of BP in LIBs, SIBs, and PIBs by ex situ XRD.<sup>[24]</sup> The results proved that the final product of lithium insertion into BP was  $\text{Li}_3\text{P}$ , the sodiation counterparts were  $\text{Na}_3\text{P}$  and  $\text{NaP}$ , and the potassiation counterparts were  $\text{K}_2\text{P}_3$ ,  $\text{KP}$ , and  $\text{K}_3\text{P}$  (Figure 2i–k). This was due to the unique binding energies of final products when phosphorus formed an alloy with lithium, sodium, and potassium (Figure 2l). In addition, the significantly lower reversible specific capacity of PIBs as compared to LIBs and SIBs also contributed to dynamic factors such as large voltage polarization and low alkali metal ion diffusion coefficient. The different discharging products resulted in the distinct capacity of P anode in AIBs.

## 2.2. $\text{M}_x\text{P}_y$

According to the reaction mechanism,  $\text{M}_x\text{P}_y$  can be divided into three categories.

Intercalation mechanism  $\text{M}_x\text{P}_y + a\text{A} = \text{A}_a\text{M}_x\text{P}_y$  (2)

The characteristic of intercalation mechanism is that the insertion of  $\text{A}^+$  does not significantly damage the structure of  $\text{M}_x\text{P}_y$  and thus maintains its cycle performance. Nevertheless, the specific capacity is relatively low. Materials for the intercalation mechanism mainly include  $\text{MnP}_4$  (7 Li, represents the “ $a\text{A}$ ” in (2)),<sup>[25]</sup>  $\text{MnP}$  (1 Li),<sup>[26]</sup>  $\text{VP}$  (1 Li),<sup>[27]</sup> and  $\text{TiP}_4$  (10.5 Li).<sup>[28]</sup> Specifically, Souza et al. prepared  $\text{MnP}_4$  with low lithium insertion potential, and its charge-discharge process was proven to be the reversible first-order topological phase transition ( $\text{MnP}_4 + 7\text{Li} = \text{Li}_7\text{MnP}_4$ ) through ex situ XRD.<sup>[25]</sup> Park et al. reported that  $\text{VP}$  showed great electrochemical performance with about 80% retention of the initial capacity (287 mA h  $\text{g}^{-1}$ ) after 250 cycles in LIBs.<sup>[27]</sup> Its reaction mechanism was demonstrated to be  $\text{VP} + \text{Li} = \text{LiVP}$  by ex situ XRD, EXAFS, and XANES (Figure 3a). Kim et al. confirmed that the mechanism for  $\text{P-TiP}_2\text{-C}$  in LIBs was intercalation rather than conversion reaction through ex situ XRD studies:  $\text{TiP}_2/\text{P}(\text{Ti}:\text{P} = 1:4) + x\text{Li} = \text{Li}_x\text{TiP}_4$ ,  $x < 12$ .<sup>[29]</sup> No alloying reaction products such as  $\text{Li}_3\text{P}$  was found, and thus its crystal structure remained stable.  $\text{P-TiP}_2\text{-C}$  showed great cycle stability of about 87% retention of the initial capacity (1116 mA h  $\text{g}^{-1}$ ) after 100 cycles.

Conversion mechanism  $\text{M}_x\text{P}_y + 3y\text{A} = y\text{A}_3\text{P} + x\text{M}$  (3)

For  $\text{M}_x\text{P}_y$  relying on the conversion mechanism, phosphorus is converted into  $\text{A}_3\text{P}$ , and the metal element, M, is dispersed as the form of nanoparticles in  $\text{A}_3\text{P}$  matrix. Although the insertion of  $\text{A}^+$  will destroy the  $\text{M}_x\text{P}_y$  structure in this case, the presence of M can help buffer the structural change and improve the conductivity of composites.  $\text{M}_x\text{P}_y$  with conversion mechanism mainly include  $\text{Cu}_3\text{P}$  ( $3 \times 1$  Li, represents the “ $3y\text{A}$ ” in (3)),<sup>[30–39]</sup>  $\text{Cu}_3\text{P}$  ( $3 \times 1$  Na),<sup>[40,41]</sup>  $\text{CuP}_2$  ( $3 \times 2$  Li),<sup>[42]</sup>  $\text{CuP}_2$  ( $3 \times 2$  Na),<sup>[43–45]</sup>  $\text{CuP}$  ( $3 \times 1$  Li),<sup>[46]</sup>  $\text{NiP}_2$  ( $3 \times 2$  Li),<sup>[47–50]</sup>  $\text{Ni}_2\text{P}$  ( $3 \times 1$  Li),<sup>[51–60]</sup>  $\text{Ni}_2\text{P}$  ( $3 \times 1$  Na),<sup>[51,59]</sup>  $\text{Ni}_5\text{P}_4$  ( $3 \times 4$  Li),<sup>[61,62]</sup>  $\text{NiP}_3$  ( $3 \times 3$  Li),<sup>[63]</sup>  $\text{NiP}_3$  ( $3 \times 3$  Na),<sup>[63]</sup>  $\text{Co}_2\text{P}$  ( $3 \times 1$  Li),<sup>[64,65]</sup>  $\text{CoP}$  ( $3 \times 1$  Li),<sup>[66–69]</sup>  $\text{CoP}$  ( $3 \times 1$  Na),<sup>[70]</sup>  $\text{CoP}_3$  ( $3 \times 3$  Li),<sup>[71,72]</sup> and  $\text{FeP}$  ( $3 \times 1$  Li),<sup>[73]</sup>  $\text{FeP}$  ( $3 \times 1$  Na),<sup>[74–79]</sup>  $\text{FeP}_2$  ( $3 \times 2$  Li),<sup>[80,81]</sup>  $\text{Fe}_2\text{P}$  ( $3 \times 1$  Li),<sup>[82]</sup>  $\text{MoP}$  ( $3 \times 1$  Na),<sup>[83]</sup>  $\text{MoP}_2$  ( $3 \times 2$  Li),<sup>[84]</sup>  $\text{V}_4\text{P}_7$  ( $3 \times 7$  Na),<sup>[85]</sup>  $\text{V}_4\text{P}_7$  ( $3 \times 7$  Li),<sup>[86]</sup>  $\text{VP}_2$  ( $3 \times 2$  Li).<sup>[87]</sup> Boyanov et al. found that the electrochemical curves of  $\text{NiP}_2$  occurred first through intercalation mechanism and then conversion mechanism ( $\text{NiP}_2 + 2\text{Li} \rightarrow \text{Li}_2\text{NiP}_2 + 4\text{Li} \rightarrow \text{Ni} + 2\text{Li}_3\text{P}$ ) through in situ XRD, NMR, and supporting DFT calculations (Figure 3b).<sup>[48]</sup> The initial intercalation stage could not destroy its structure obviously, resulting in great stability. However, the subsequent conversion process damaged its structure completely with the dispersion of Ni nanoparticles in  $\text{Li}_3\text{P}$  matrix, bringing about the poor cycling performance

Alloy mechanism  $\text{M}_x\text{P}_y + (3y + bx)\text{A} = y\text{A}_3\text{P} + x\text{A}_b\text{M}$  (4)

The trait of  $\text{M}_x\text{P}_y$  in which the alloy mechanism dominates is that in addition to the conversion of phosphorus into  $\text{A}_3\text{P}$ , M is also alloyed to produce  $\text{A}_b\text{M}$ . The  $b$  value can be obtained from the phase diagram of A–M binary alloy. Although the insertion of  $\text{A}^+$  will completely destroy the structure of  $\text{M}_x\text{P}_y$ , these materials have the highest capacity among all metal phosphides.  $\text{M}_x\text{P}_y$  with the alloy mechanism mainly include  $\text{Sn}_4\text{P}_3$  ( $3 \times 3 + 15/4 \times 4$  Na, represents the “ $(3y + bx)\text{A}$ ” in (4)),<sup>[88–92]</sup>  $\text{Sn}_4\text{P}_3$  ( $3 \times 3 + 1 \times 4$  K),<sup>[93]</sup>  $\text{Sn}_4\text{P}_3$  ( $3 \times 3 + 4 \times 4$  Li),<sup>[94,95]</sup>  $\text{SnP}_3$  ( $3 \times 3 + 15/4 \times 1$  Na),<sup>[96,97]</sup>  $\text{GeP}_5$  ( $3 \times 5 + 22/5 \times 1$  Li),<sup>[98]</sup>  $\text{GeP}_5$  ( $3 \times 5 + 1 \times 1$  Na),<sup>[99,100]</sup>  $\text{Ge}_2\text{P}_3$  ( $3 \times 3 + 2 \times 22/5$  Li),<sup>[101]</sup>  $\text{Ge}_2\text{P}_3$  ( $3 \times 3 + 1 \times 2$  Na),<sup>[101]</sup>  $\text{GeP}_3$  ( $3 \times 3 + 1 \times 22/5$  Li),<sup>[102]</sup>  $\text{GeP}_3$  ( $3 \times 3 + 1 \times 1$  Na),<sup>[103]</sup>  $\text{InP}$  ( $1 \times 1 + 13/3 \times 1$  Li),<sup>[104]</sup>  $\text{ZnP}_2$  ( $2 \times 3 + 1 \times 1$  Li),<sup>[105–107]</sup>  $\text{Zn}_3\text{P}_2$  ( $2 \times 3 + 1 \times 3$  Li),<sup>[108,109]</sup>  $\text{SiP}_2$  ( $2 \times 3 + 1 \times 15/4$  Li),<sup>[110]</sup>  $\text{Se}_4\text{P}_4$  ( $4 \times 3 + 4 \times 2$  Na).<sup>[111]</sup> For instance, Qian et al. discovered that  $\text{Sn}_4\text{P}_3$  went through the alloy mechanism ( $\text{Sn}_4\text{P}_3 + 24\text{Na} \rightarrow \text{Na}_{15}\text{Sn}_4 + 3\text{Na}_3\text{P}$ ) through ex situ XRD, and it exhibited great electrochemical performance with  $\approx 86\%$  retention of the initial capacity (850 mA h  $\text{g}^{-1}$ ) after 150 cycles. The great electrochemical performance was attributed to the fast electron transport channels provided by intermediate Sn nanoparticles, and, moreover, the agglomeration of Sn could be prevented by using  $\text{Na}_3\text{P}$  as a matrix (Figure 3c). Lu et al. revealed that  $\text{Se}_4\text{P}_4$  underwent the three-step reaction process ( $\text{Se}_4\text{P}_4 \rightarrow \text{Na}_x\text{Se}_4\text{P}_4 \rightarrow \text{Na}_2\text{Se} + \text{P} \rightarrow \text{Na}_2\text{Se} + \text{Na}_3\text{P}$ ).<sup>[111]</sup> The first stage occurred through the intercalation mechanism, and the second and third steps went through the alloying reaction of Se and P, respectively (Figure 3d). The first-cycle specific capacity of material was close to its theoretical value (1048 vs 1217 mA h  $\text{g}^{-1}$ ), which was ascribed to the synergistic effect of Se and P.

Generally, if M cannot be alloyed with A and the structure of  $\text{M}_x\text{P}_y$  contains the vacancy for embedding  $\text{A}^+$ ,  $\text{M}_x\text{P}_y$  will employ the intercalation mechanism. If M cannot be alloyed with A and  $\text{M}_x\text{P}_y$  does not possess vacancy for  $\text{A}^+$ ,  $\text{M}_x\text{P}_y$  will display

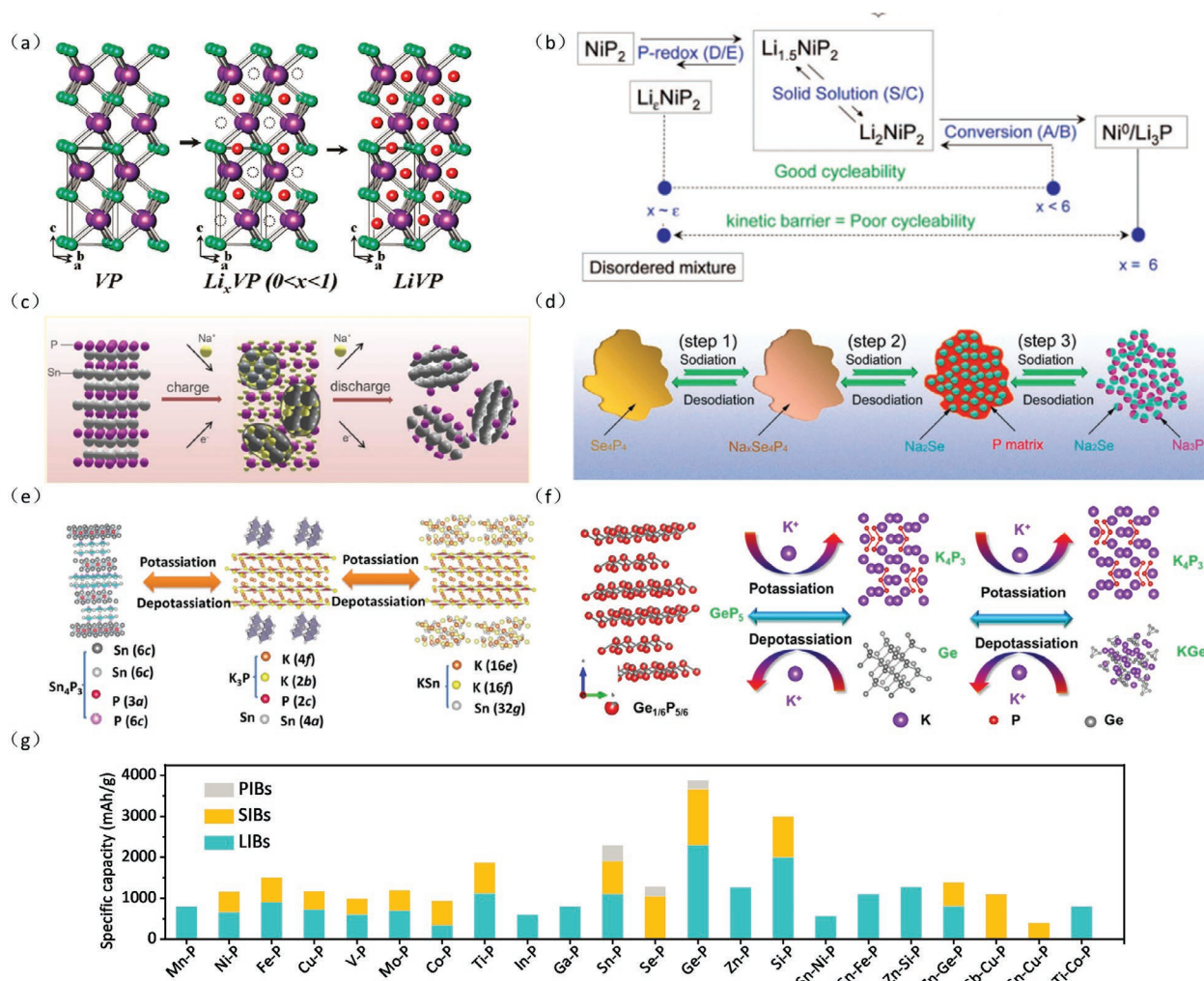


**Figure 3.** Alkaline metal ions storage mechanisms of  $M_xP_y$  in AIBs: a) Suggested topotactic reaction mechanism of VP; b) Redox mechanism of  $NiP_2$  electrode; c) Schematic illustration of the Na-storage mechanism in  $Sn_4P_3$  electrode; d) Schematic illustration for the mechanism of  $Se_4P_4$  during sodiation/depotassiation; e) The potassiation/depotassiation process in  $Sn_4P_3$  electrode; f) Schematic illustration of the potassiation/depotassiation process in  $GeP_5$  electrode; g) Summary of  $M_xP_y$  with various specific capacity in literature. a) Reproduced with permission.<sup>[27]</sup> Copyright 2009, American Chemical Society. b) Reproduced with permission.<sup>[48]</sup> Copyright 2009, American Chemical Society. c) Reproduced with permission.<sup>[121]</sup> Copyright 2014, American Chemical Society. d) Reproduced with permission.<sup>[111]</sup> Copyright 2016, Wiley-VCH. e) Reproduced with permission.<sup>[93]</sup> Copyright 2017, American Chemical Society. f) Reproduced with permission.<sup>[121]</sup> Copyright 2018, Elsevier.

the conversion mechanism.<sup>[112]</sup> When M can be alloyed with A,  $M_xP_y$  will be demonstrated the alloy mechanism. According to reaction characteristics, the theoretical specific capacity of  $M_xP_y$  can be ranked by their mechanism, namely, as intercalation < conversion < alloy, and the volume expansion is ranked similarly. That is to say, the larger capacity, the greater volume expansion and thus the shorter cycle life. Therefore, it is essential to find the balance between capacity and cycle life to determine the appropriate types of  $M_xP_y$ .

In addition to binary alloys, multielement alloy is commonly ternary alloys including Sn-Ni-P,<sup>[113]</sup> Sn-Fe-P,<sup>[114]</sup> Sn-Cu-P,<sup>[115]</sup> Zn-Ge-P,<sup>[116]</sup> and Sb-Cu-P,<sup>[117]</sup> Sb-Fe-P,<sup>[118]</sup> Ti-Co-P,<sup>[119]</sup> and their ion storage mechanisms are similar to those of binary alloys. For example, Li et al. synthesized  $ZnSiP_2/C$  with ordered and disordered cations, respectively, and its charge-discharge mechanism was  $ZnSiP_2 \rightarrow Li_2ZnSiP_2 \rightarrow Li_{4.4}Si + LiZn + Li_3P$ .<sup>[120]</sup> The results showed that disordered materials exhibited better

electrochemical properties. The capacity retention after 2000 cycles was 84.6% ( $1500 \text{ mA h g}^{-1}$ ), which was attributed to the higher conductivity and smaller volume expansion of the disordered material. Figure 3g summarizes  $M_xP_y$  with various specific capacity in literature.

It should be noted that the  $A_3P$  in reactions (3) and (4) is best suited to LIBs and SIBs, and less so for PIBs because of uncertain discharge products (e.g.,  $K_3P$ ,  $KP$ ,  $K_4P_3$ ,  $K_3P$ ). Even so, the reaction mechanism of  $M_xP_y$  in PIBs can also draw lessons from LIBs and SIBs. For example,  $GeP_5$  ( $3GeP_5 + 23K \leftrightarrow 5K_4P_3 + 3KGe$ ) (Figure 3f),<sup>[121]</sup>  $Sn_4P_3$  ( $Sn_4P_3 + 13K \leftrightarrow 3K_3P + 4KSn$ ) (Figure 3e)<sup>[93]</sup> and  $Se-2P$  ( $3Se - 2P + 7K \leftrightarrow 2K_2P_3 + 3KSe$ )<sup>[122]</sup> display an analogous alloy mechanism in PIBs.

Due to the similarities in synthesis, challenges, and corresponding strategies between P anodes and  $M_xP_y$ , the latter chapter does not separate them in to different sections, rather they are discussed as separate paragraphs.

### 3. Scientific and Technical Challenges

Despite the high specific capacity of P anode under alloy reaction mechanism, it also faces many challenges. 1) The stress produced in the process of multi-electron transfer reaction will lead to the huge volume change in phosphorus ( $\approx 300\%$  in LIBs and  $\approx 400\%$  in SIBs). After many cycles, phosphorus particles will be pulverized, and the electrode loses both its integrity and electrical contact with current collector (Figure 4a). 2) The great volume change means that phosphorus anodes will continuously generate fresh surfaces during cycling, causing the decomposition of electrolyte to generate unstable solid electrolyte interphase (SEI). This process will also consume  $A^+$  ions and seriously affect cycle life of full cell, and the gradually thickened SEI will increase the interface impedance. 3) The poor conductivity of phosphorus will cause sluggish kinetics (Figure 4b).

In addition to the above scientific issues, there are also some technical challenges. 1) Due to the high reactivity of phosphorous, especially nano-phosphorous, their surface is easily oxidized to form a passivation layer (such as  $P_2O_5$ ) in air, which reduces electrochemical performance greatly (Figure 4d).<sup>[123]</sup> 2) When phosphorous is prepared under high temperature or pressure, WP will inevitably be formed, and its easy self-ignition may create serious safety hazards (Figure 4c).<sup>[124]</sup>

3) Because phosphorus can react with copper at high temperature, there may be risks when copper film is used as the anode current collector (Figure 4e).<sup>[125]</sup>

The scientific and technical challenges in P anode are also partially suitable for  $M_xP_y$  anodes. As mentioned in Section 2.2, the volume expansion of  $M_xP_y$  depends on the specific reaction mechanism.  $M_xP_y$  with an alloying mechanism shows the largest volume change and thus the most unstable SEI, while the relatively solid structure of  $M_xP_y$  with an intercalation mechanism operating, results in better cycling performance. Although the conductivity of  $M_xP_y$  depends on the type of metal, generally speaking, its value is better than that of pure phosphorus due to the introduction of a metal. Technical challenges including safety hazards, high activity in air and incompatibilities with Cu current collectors in P anode systems can be alleviated with  $M_xP_y$  due to a lack of active phosphorus.

### 4. Advanced Synthesis Methods

#### 4.1. High-Energy Ball Milling (HEBM) Method

HEBM is the most commonly used method to synthesize phosphorus-based materials and characterized by its high efficiency.

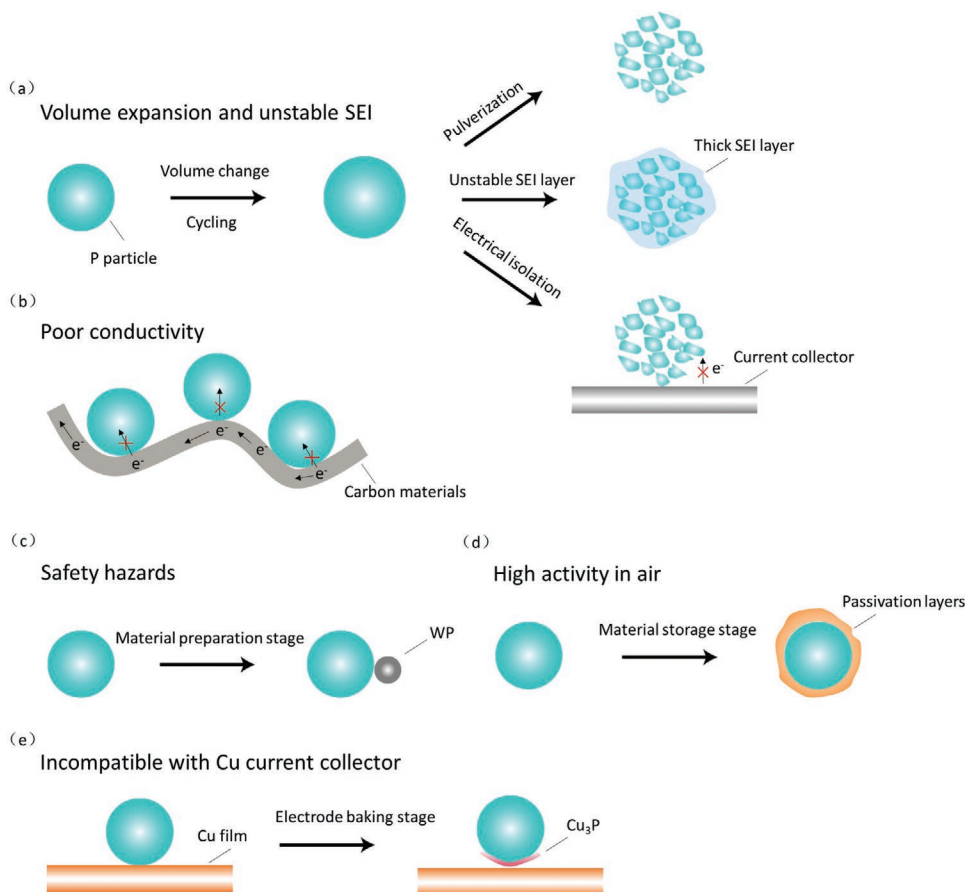


**Figure 4.** Scientific challenges and technical issues for P anodes in AIBs: a) Huge volume expansion and unstable SEI; b) Poor conductivity; c) Safety hazards; d) High activity in air; e) Incompatible with Cu current collector.

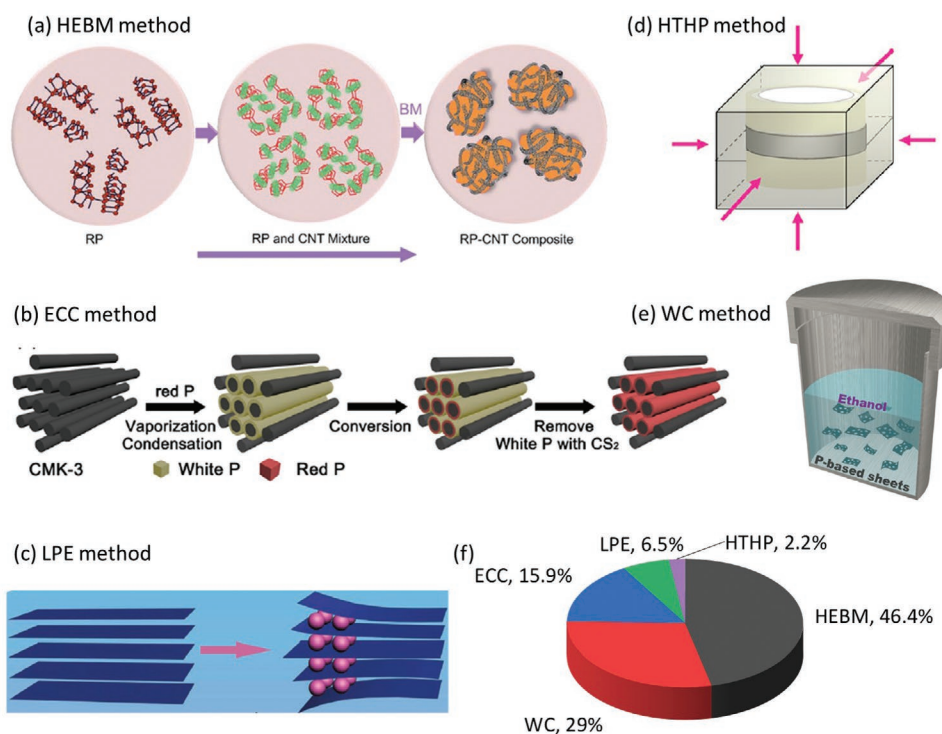


**Figure 5.** Advanced synthesis methods: a) Schematic of high-energy ball milling (HEBM) methods to synthesize RP-carbon composites; b) Schematic of evaporation condensation conversion (ECC) methods to synthesize P@CMK-3 composites; c) Schematic of liquid phase exfoliation (LPE) methods to produce phosphorene; d) Schematic of high temperature and pressure (HTHP) methods to produce BP; e) Schematic of wet chemical (WC) methods for the formation of phosphorus-based materials; f) Ratio of various methods for the preparation of phosphorus-based materials in literature. a) Reproduced with permission.<sup>[126]</sup> Copyright 2018, Royal Society of Chemistry. b) Reproduced with permission.<sup>[127]</sup> Copyright 2016, American Chemical Society. c) Reproduced with permission.<sup>[132]</sup> Copyright 2017, Wiley-VCH. d) Reproduced with permission.<sup>[129]</sup> Copyright 2012, American Chemical Society. e) Reproduced with permission.<sup>[134]</sup> Copyright 2016, Wiley-VCH.

It is suitable for not only preparing materials with small particle size but also changing crystal form and even the creation of new phases (Figure 5a).<sup>[126]</sup> For HEBM, the rotation and revolution of bowls make samples collide at ultra-high speed with balls and the wall, which produces impact, shear, and grinding forces for sample mixing. The ball milling speed, time, and ball-to-material ratio are the most important parameters for controlling the preparation efficiency. Generally speaking, higher rotation speed, longer milling time, and larger ball-to-material ratios will improve the synthesis efficiency. Besides, considering the fact that RP (is usually used as raw material) is easily oxidized during HEBM, ball milling devices should be kept in a glove box or continuously filled with inert gas. Compared with the original RP, products of HEBM show higher activity and therefore should be stored in the glove box for safety reasons.

#### 4.2. Heat Treatment Methods

Although HEBM is very convenient for the preparation of phosphorus-based materials, it does not completely package phosphorous into the carbon coating layer. Due to the low sublimation temperature of RP (419 °C), the method of evaporation condensation conversion (ECC) can be used to prepare phosphorus/carbon composites (P/C) with RP confined in porous carbon materials (Figure 5b).<sup>[127]</sup> During experiments, RP is

usually heated above the sublimation temperature in inert atmosphere to make RP vapor diffuse into carbon channels. In the subsequent condensation process, RP will first be converted into WP, and after remaining at constant temperature at about 250 °C for a period of time, WP will transform into RP again. After cooling to room temperature, it is necessary to use CS<sub>2</sub> to remove residual WP on the surface of porous carbon. ECC can effectively confine RP in porous carbon, improve the conductivity of composites, and restrain the volume change of RP during charge and discharge. However, the use of toxic CS<sub>2</sub> makes scale-up difficult.

Heat treatment methods can even be used to synthesize M<sub>x</sub>P<sub>y</sub> which is difficult to be synthesized by HEBM. For example, Nazar and co-workers prepared MnP<sub>4</sub> successfully by the tin-flux technique under high temperature with powders of Mn, P and Sn as raw materials.<sup>[25]</sup> Tin powder as the reaction medium can reduce the activation energy because of its low melting point (231 °C). A reaction based on a similar principle can also be used to synthesize MnP<sub>4</sub> with Mn, P and I<sub>2</sub> as the raw materials.<sup>[128]</sup>

#### 4.3. High Temperature and High Pressure (HTHP) Methods

High temperature and pressure are necessary conditions for synthesizing BP from RP. Albeit BP can be synthesized by

HEBM because the procedure creates local high temperature and pressure spots, this method shows poorly controlled manner. In fact, the temperature and pressure conditions for converting RP to BP can be systematically explored by using the HTHP method (Figure 5d). Sun et al. found that the best temperature and pressure for converting RP to BP were 800 °C and 4.5 GPa, respectively.<sup>[129]</sup> Similar to the heat treatment method, HTHP can also be applied to synthesize phosphorus-rich  $M_xP_y$  including  $MnP_4$ ,  $FeP_4$  and  $CrP_4$ .<sup>[130]</sup>

#### 4.4. Liquid Phase Exfoliation Methods

BP is the layered material which is similar to graphite, connected by strong covalent bonds within the layer and weak van der Waals force between layers.<sup>[131]</sup> Therefore, BP can be transformed into the 2D phosphorene with a few layers of phosphorus atoms by LPE methods (Figure 5c).<sup>[132]</sup> LPE mainly uses foreign ions or solvent molecules to peel layered materials into 2D sheets under the action of agitation or ultrasound (mainly through ion intercalation, ion exchange, and ultrasound-assisted LPE). It is worth noting that the solvent used in LPE is vital, since the solvent with proper surface energy can prevent 2D materials from reuniting. Common solvents include N-methyl pyrrolidone (NMP), isopropyl alcohol (IPA), and N,N-dimethylformamide (DMF).<sup>[133]</sup>

#### 4.5. Wet Chemical (WC) Methods

In addition to the above, phosphorus-based materials can be synthesized by various wet chemical (WC) methods (Figure 5e). For example, Zhang et al. used a solvothermal method to synthesize RP nanosheets, with RP as raw materials and ethanol as solvent.<sup>[134]</sup> During the synthesis process, bulk RP was transformed from solid to gas and then backed to solid state in the evaporation condensation procedure, and finally successfully converted into phosphorous nanosheets by bottom-up process. Zhou et al. prepared hollow porous phosphorus nanospheres directly through the chemical reaction of  $10NaN_3 + 2PCl_3 \xrightarrow{\text{Toluene}} 2P + 10NaCl + 15N_2$ .<sup>[135]</sup> This special structure helped to buffer the volume change of phosphorous, thereby improving its cycle stability. Yu and co-workers synthesized uniform yolk-shell  $Sn_4P_3@C$  nanospheres through a multistep hydrothermal route. The composites exhibited a high capacity and long cycling life in SIBs.<sup>[92]</sup> Figure 5f summarizes common methods for the preparation of phosphorus-based materials in literature.

## 5. Corresponding Strategies for Meeting Challenges

### 5.1. Nanomaterials Preparation

As mentioned in Section 4.4, BP can be converted into phosphorene with a thickness of only a few atomic layers by LPE. Phosphorene is usually further compounded with other 2D materials such as graphene,<sup>[136]</sup> MAXene and transition metal

dichalcogenides (TMDs) to increase the conductivity and buffer volume expansion of the phosphorus. For instance, Jain et al. prepared phosphorene, phosphorene/CNTs composites, and phosphorene/graphene composites by LPE using NMP as solvent (Figure 6a).<sup>[137]</sup> Electrochemical results showed that the phosphorene/graphene composites exhibited the best cycling performance in PIBs with a capacity retention of  $\approx 74\%$  after 50 cycles. This was attributed to the graphene with its 2D structure allowing it to better support 2D phosphorene. Meng et al. synthesized black phosphorus quantum dots (BPQDs) and  $Ti_3C_2$  nanosheets (TNSs) composites by LPE, and P–O–Ti interfacial bonds were demonstrated between the two components (Figure 6b).<sup>[138]</sup> BPQDs/TNSs exhibited excellent electrochemical performance in LIBs with a capacity retention of more than 100% after 2400 cycles. This was due to the dual-model energy storage (DMES) mechanism of the composites, in which BPQDs displayed battery mechanism and TNSs represented a pseudocapacitor mechanism.

The preparation of phosphorene by LPE is only suitable for the modification of BP. For RP and  $M_xP_y$ , various nanostructures such as hollow structures,<sup>[139]</sup> porous structures,<sup>[76,140]</sup> yolk-shell structures<sup>[92,141,142]</sup> and layered structures they can be synthesized by varieties of wet chemical methods to buffer the volume change of composites. For example, Liu et al. prepared honeycomb phosphorus-rich  $CuP_2$  using a low-temperature molten salt approach with  $ZnCl_2$  (its melting point is only about 290 °C) as reaction medium, and the composites displayed great electrochemical performance in LIBs with a specific capacity of 720 mA h  $g^{-1}$  after 600 cycles (Figure 6c).<sup>[143]</sup> The phosphorus-rich  $CuP_2$  and honeycomb porous structure resulted in a high capacity and increased structural stability.

### 5.2. Carbon Coating

The introduction of carbon materials not only improves the conductivity of P anode and  $M_xP_y$  but also buffers their volume change, so as to enhance the rate performance and cycle life of composites. Generally, when preparing P/C, the following three aspects need to be designed carefully.

#### 5.2.1. The Mass Ratio of Phosphorus to Carbon

Owing to the similar electrochemical windows of phosphorus and carbon materials, both contribute to specific capacity of P/C.

$$\begin{aligned} Q_{P/C} &= Q_P \times R_P + Q_C \times R_C \\ &= 2590 \times (1 - R_C) + Q_C \times R_C \\ &= 2590 - R_C(2590 - Q_C) \end{aligned} \quad (5)$$

Where  $Q_{P/C}$  is the specific capacity of P/C in mA h  $g^{-1}$ ,  $Q_P$  is the theoretical specific capacity of phosphorus (2590 mA h  $g^{-1}$ ),  $R_C$  is the mass ratio of carbon ( $R_C = \frac{M_C}{M_P + M_C}$ , where  $M_P$  and  $M_C$  represent the mass of phosphorus and carbon in composites, respectively).  $R_P$  is the mass ratio of phosphorus ( $1 - R_C$ ), and  $Q_C$

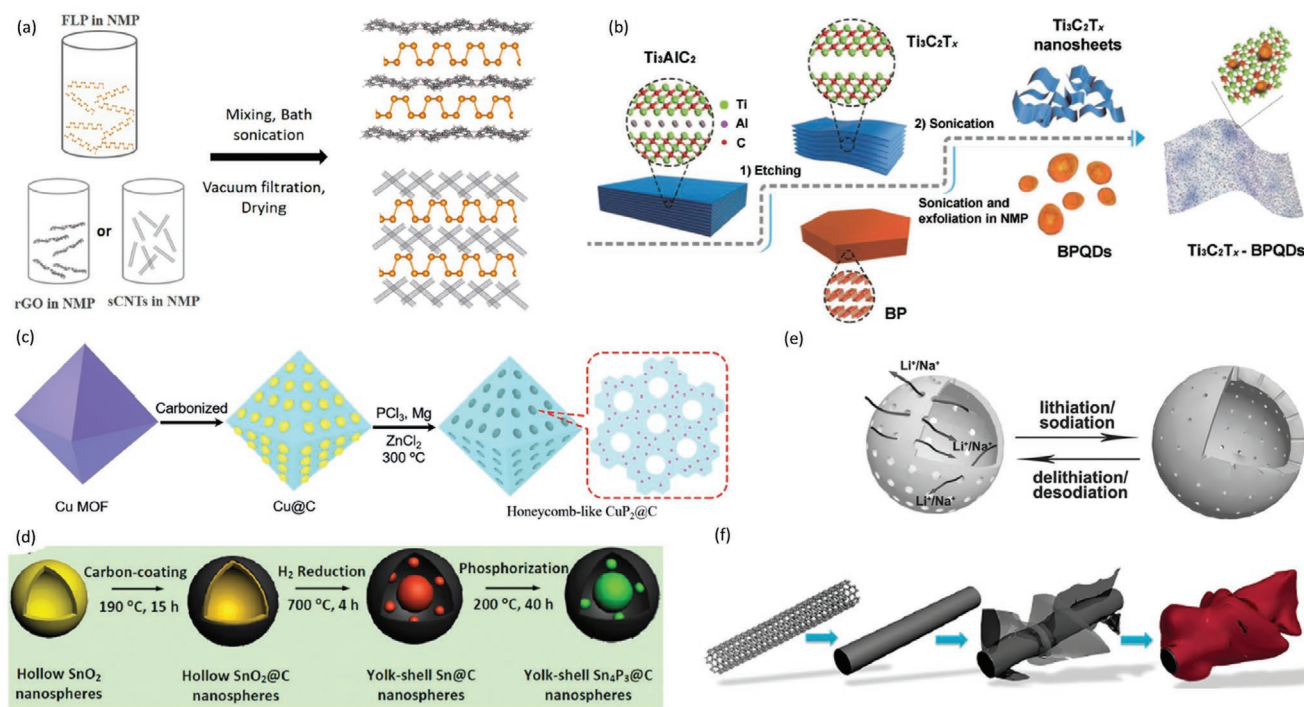


**Figure 6.** Nano-materials preparation: a) Illustration of fabrication of phosphorene/rGO and phosphorene/sCNTs; b) Illustration of the synthesis of the BPQD/TNS composite; c) Illustration of the preparation of a honeycomb  $Cu_2@C$  nanostructure; d) Illustration of the synthesis of yolk-shell  $Sn_4P_3@C$  nanosphere anodes; e) Illustration of hollow nanospheres with porous shells during charge and discharge process; f) Illustration of the synthesis of  $SiC@graphene@P$ . a) Reproduced with permission.<sup>[137]</sup> Copyright 2019, American Chemical Society. b) Reproduced with permission.<sup>[138]</sup> Copyright 2018, Wiley-VCH. c) Reproduced with permission.<sup>[143]</sup> Copyright 2019, Wiley-VCH. d) Reproduced with permission.<sup>[92]</sup> Copyright 2015, Royal Society of Chemistry. e) Reproduced with permission.<sup>[135]</sup> Copyright 2017, Wiley-VCH. f) Reproduced with permission.<sup>[203]</sup> Copyright 2017, American Chemical Society.

is the theoretical specific capacity of carbon, therefore,  $Q_{P/C}$  is determined by the type of carbon material ( $Q_C$ ) and  $R_C$ . Generally speaking,  $Q_C < Q_P$ , so the larger  $R_C$ , the smaller  $Q_{P/C}$ . On the other hand, because carbon material shows less volume expansion than phosphorus, a larger  $R_C$  reduces the volume expansion and enhances the conductivity of P/C, and thus the cycle and rate performance will be improved. Therefore,  $R_C$  should be determined by balancing specific capacity against cycle performance. For example, Xu et al. prepared a series of phosphorus-graphite composites by HEBM (denoted as  $x$  P- $\gamma$  C, the mass ratio of P/C =  $x/\gamma$ ,  $x + \gamma = 10$ ), and explored their electrochemical behavior in LIBs.<sup>[144]</sup> When  $\gamma = 0$  (pure RP), the first discharge capacity and initial Coulombic efficiency was  $449 \text{ mA h g}^{-1}$  and 5.1%, respectively. This showed that RP which did not compound with carbon exhibited rather low electrochemical performance. When  $x = 0$  (pure graphite), the first discharge capacity was  $1105.4 \text{ mA h g}^{-1}$ , and there was no typical charging and discharging platform ( $\approx 0.2 \text{ V vs Li/Li}^+$ ) belonging to graphite. This could be explained by the layered structure of graphite was destroyed during HEBM process, and thus the electrochemical behavior resembled that of disordered carbon materials such as hard carbon and soft carbon. When  $0 < x < 10$ , the smaller  $x$  was, the more similar the electrochemical curves of  $x$  P- $\gamma$  C were close to disordered carbon materials. Among them, 6 P-4 C and 3 P-7 C displayed the best comprehensive performance, which was attributed to the synergistic effect of phosphorus and graphite to generate stable SEI and limit the volume expansion.

## 5.2.2. Types of Carbon Materials

Carbon materials commonly used in P/C can be classified into 0D  $C_{60}$  and carbon black (CB),<sup>[145–154]</sup> 1D carbon nanotubes (CNTs)<sup>[153,155–162]</sup> and carbon nanofibers (CNFs),<sup>[17,163–165]</sup> 2D graphene,<sup>[166–179]</sup> and 3D porous carbon<sup>[180–186]</sup> and graphite.<sup>[187,188]</sup> The type of carbon material affects properties of P/C in the following ways. First, different kinds of carbon materials have various  $Q_C$ , which will influence the value of  $Q_{P/C}$ . Second, the type of carbon material determines its conductivity, and nanocarbons such as CNTs and graphene have much higher conductivity and help the rate performance of P/C. Third, since 1D CNTs have high aspect ratio and the 2D graphene has large lateral size, these materials have the ability to connect different phosphorus particles to build a complete conductive network. For example, Li et al. prepared composites of RP and CNTs (RP-CNTs) by simple hand grinding, and the product showed better electrochemical performance than RP-CB composites.<sup>[160]</sup> Those authors ascribed it to the fact that CNTs could not only buffer the volume change and prevent the aggregation of phosphorus particles, but also help to form a conductive network (Figure 7b). Similarly, Zhou et al. prepared phosphorus-CNTs-graphene composites by a WC method to build the complete conductive 3D network, so that the material could function in both LIBs and SIBs with excellent electrochemical performance (Figure 7d).<sup>[171]</sup> Sun et al. successfully confined RP in porous carbon by ECC method.<sup>[189]</sup> This approach not only improved the conductivity of materials, but

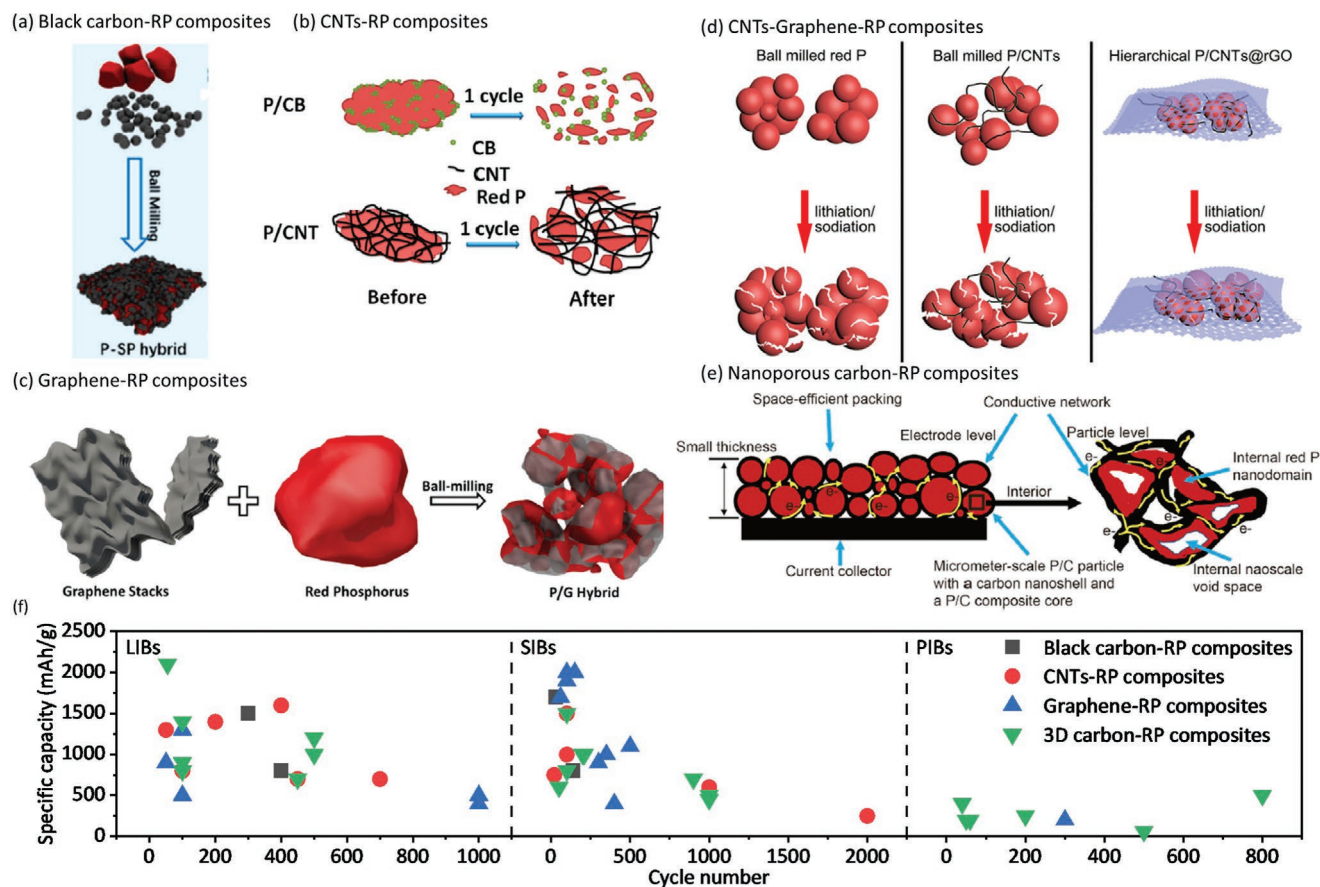


**Figure 7.** P/C preparation: a) Schematic diagram for Black carbon-RP composites; b) Proposed function of CNTs during the volume expansion; c) Schematic illustration of the synthesis of Graphene-RP composites; d) Schematic illustration of different RP hybrids before and after lithiation or sodiation; e) Structural design of nanoporous carbon-RP composites; f) Summary of P/C with various specific capacity and cycle numbers in literature. a) Reproduced with permission.<sup>[195]</sup> Copyright 2019, American Chemical Society. b) Reproduced with permission.<sup>[160]</sup> Copyright 2013, American Chemical Society. c) Reproduced with permission.<sup>[176]</sup> Copyright 2014, American Chemical Society. d) Reproduced with permission.<sup>[171]</sup> Copyright 2018, Elsevier. e) Reproduced with permission.<sup>[189]</sup> Copyright 2019, Elsevier.

also limited its volume expansion, realizing the high loading of active materials ( $3.5 \text{ mA h cm}^{-2}$ ) and great rate performance (8C) (Figure 7e). Fourthly, the interaction between carbon and phosphorus will vary according to the types of carbon materials. Sun et al. proved that compared with  $\text{C}_{60}$ , oxide graphite, and CB, graphite could form more P–C bonds with phosphorus, thus improving the cycle performance of composites mainly due to the relatively stable  $\text{sp}^2$  P–C bond.<sup>[121]</sup>

### 5.2.3. Ball Milling Parameters

Under fixed ball-to-material ratio and rotation speed, the longer milling time generally produces P/C with the smaller particle size and stronger interaction between carbon and phosphorus, while the synthesis efficiency will be reduced. Consequently, it is necessary to select the appropriate milling parameters. Furthermore, these parameters also affect the conversion efficiency from RP to BP. Ferrara et al. studied the effect of rotation speed, milling time, and ball-to-material ratio on the conversion efficiency, and found the last factor to be the most critical.<sup>[190]</sup> When the ball-to-material ratio and rotation speed was 110:1 and 500 rpm

respectively, only 15 min was needed to completely convert RP to BP. It should be noted that, in addition to milling parameters, the synthesis of BP from RP by HEBM is also affected by the type of raw materials.<sup>[126]</sup> Specifically, when raw materials was just pure RP, BP could be produced by adjusting ball milling parameters. However, if raw materials were the mixture of RP and carbon materials, only composites of RP and carbon could be obtained instead of BP. This was mainly because the added carbon material would consume a part of ball milling energy, so that RP could not be converted into BP. Figure 7f summarize P/C with various specific capacity and cycle life in literature.

Carbon coating is also an interesting strategy with which to enhance the conductivity of  $\text{M}_x\text{P}_y$ , and design principles about the types and ratio of carbon material in  $\text{M}_x\text{P}_y/\text{carbon}$  composites ( $\text{M}_x\text{P}_y/\text{C}$ ) can be extracted from examples with P/C. Various types of carbon materials have been used to combine with  $\text{M}_x\text{P}_y$ , including carbon black,<sup>[42,44]</sup> CNTs,<sup>[76]</sup> graphene<sup>[43,51,52,58,59,73,90,91,191,192]</sup> and porous carbon.<sup>[68]</sup> Lou et al. prepared monodispersed carbon-coated cubic  $\text{NiP}_2$  nanoparticles anchored on carbon nanotubes ( $\text{NiP}_2@\text{C-CNTs}$ ) through a series of steps, which included refluxing, annealing, reduction, carbon coating, and phosphorization.<sup>[47]</sup> The composites exhibited an

excellent electrochemical performance with a specific capacity of 650 mA h g<sup>-1</sup> after 1500 cycles, owing to the fact that the carbon coating could prevent the NiP<sub>2</sub> nanoparticles agglomerating while the CNTs helped buffer volume change and improved conductivity. Bai et al. employed a self-template and -assembly approach to prepare CoP nanoparticles embedded into nitrogen and phosphorus co-doped porous carbon sheets, which exhibited a good capacity retention in both LIBs (500 mA h g<sup>-1</sup> after 800 cycles) and PIBs (200 mA h g<sup>-1</sup> after 1000 cycles).<sup>[67]</sup> The excellent performance was attributed to its unique hierarchical structure, a high specific surface area, and porous features which could help buffer the volume expansion of CoP.

In addition to enhancing conductivity, the introduction of carbon material may also change the crystal form of M<sub>x</sub>P<sub>y</sub>. For example, Li et al. first synthesized ZnP<sub>2</sub> and Zn<sub>3</sub>P<sub>2</sub> by ball milling, and then mixed them with graphite in the same proportion.<sup>[193]</sup> ZnP<sub>2</sub> was found to be transformed into amorphous ZnP<sub>2</sub>/C composites, while Zn<sub>3</sub>P<sub>2</sub> was converted into 3Zn-2P/C composites with a phase separation of Zn and P. The reaction mechanism of amorphous ZnP<sub>2</sub>/C was ZnP<sub>2</sub> → Li<sub>x</sub>ZnP<sub>2</sub> → LiZn + Li<sub>3</sub>P. ZnP<sub>2</sub>/C, which showed better electrochemical performance with 83% retention of the initial capacity (1500 mA h g<sup>-1</sup>) after 2730 cycles. This was mainly due to the isotropic stress produced by the amorphous structure of materials, which inhibited material pulverization.

### 5.3. Functional Electrolytes and Binders Exploration

When anode materials are discharged to low potential (≈1.2 V vs Li/Li<sup>+</sup> in LIBs), electrolyte in batteries will be decomposed. The generated solid products could be deposited on the surface of anode to form a porous film called SEI. Although SEI can conduct ions and block electrons to broaden the electrochemical window of electrolyte, it also consumes active A<sup>+</sup> and increases the interface impedance.<sup>[194]</sup> The alloy reaction mechanism of phosphorus causes huge volume changes, and thus phosphorus particles will be pulverized constantly, forming an unstable SEI.

The properties of SEI are closely related to the composition of electrolyte, which mainly consists of inorganic salt, organic solvent, and electrolyte additives. Lei et al. found that adding 10% fluoroethylene carbonate (FEC) to carbonate electrolyte could significantly improve the cycling performance of P/C in LIBs.<sup>[195]</sup> This was mainly due to the fact that FEC showed lower LUMO energy levels than ethylene carbonate (EC) and diethyl carbonate (DEC) and thus preferentially decomposed during discharge, which helped increase the content of F in SEI, especially that of LiF (Figure 8a,b). LiF had the following functions: 1) As an electronic insulator, it inhibited further decomposition of the electrolyte. 2) Its porous structural features could accelerate the migration of Li<sup>+</sup> in SEI. 3) Being more stable than other organic components, and thus it enhanced the stability of SEI. Naoaki and co-workers used FEC and vinylene carbonate (VC) to improve the cycling performance of P/C in SIBs, and compared their differences in mechanism.<sup>[196]</sup> They found that FEC primarily increased the content of inorganic components such as NaF in SEI, while VC mainly raised the content of polymers, and both effects were conducive to the formation of stable SEI (Figure 8c,d,i).

Electrolyte also plays a key role in promoting the stability of SEI in M<sub>x</sub>P<sub>y</sub>, especially these with alloy mechanism. Using theoretical calculations, Zhang et al. found that the solvation energy of K<sup>+</sup> in EC/DEC was lower than that in EC/DEC/FEC.<sup>[121]</sup> Therefore, K<sup>+</sup> was easier to desolve in EC/DEC, and the ion diffusion resistance could be low (Figure 8e). In addition, they also studied the SEI on GeP<sub>5</sub> using in situ infrared spectroscopy imaging, and proved that potassium bis(fluorosulfonyl)imide (KFSI) could generate thinner and more uniform SEI than KPF<sub>6</sub> did, while the addition of FEC increased the thickness of SEI and destroyed its uniformity (Figure 8f). It is worth noting that these conclusions are just opposite to the effect of FEC in P/C.

Although the mass ratio of binder used in batteries is limited, it's critical for maintaining the integrity of electrode structure and thus forming the continuous conduction path of electrons and ions.<sup>[197]</sup> However, traditional polyvinylidene fluoride (PVDF) binder is not suitable for electrode materials exhibiting large volume expansion (including silicon, phosphorus, and tin-based materials) due to its low adhesion strength and poor stability. For this reason, many new water-based binders such as carboxymethyl cellulose (CMC), CMC-styrene butadiene rubber (SBR), polyacrylic acid (PAA), sodium alginate (SA), and polyimide (PI) have been proposed. These binders are rich in carboxyl or hydroxyl groups that can form chemical bonds with oxygen-containing functional groups on the surface of materials to improve adhesion. Naoaki et al. reported that when using traditional PVDF binder, the discharge capacity of material could be close to its theoretical value, while the charge capacity was minute mainly because of the huge volume change of phosphorus during discharge.<sup>[198]</sup> The use of sodium polyacrylate (PANA) as binder could significantly enhance its electrochemical performance, due to the binder's high adhesion, the ability to evenly disperse active materials, and great compatibility with electrode materials (Figure 8j). In addition, some conventional binders can be cross-linked and polymerized to form polymers with higher molecular weight and richer functional groups to improve their adhesion strength. For example, Song et al. observed esterification between carboxyl group on citric acid (CA) and hydroxyl group on CMC to form a functional CA-CMC binder.<sup>[199]</sup> CA-CMC could bond with oxidized CNTs and phosphorus composite to maintain the integrity of electrode materials and improve cycle performance of battery (Figure 8k). Figure 8l summarize electrolyte solvents, additives and binders used for phosphorus-based anode in literature.

### 5.4. Electrochemical Window Regulation

The volume expansion of P anodes is proportional to the specific capacity, so cycling performance can be improved by narrowing its electrochemical window. For example, Park et al. compared RP, BP and BP/C composites, and found that the composites exhibited the highest Coulombic efficiency.<sup>[146]</sup> The multistep alloying reaction mechanism was further revealed by ex situ XRD studies, and the cycle stability could be effectively improved by increasing its lower limit potential.

This method is also applicable to M<sub>x</sub>P<sub>y</sub>. In fact, M<sub>x</sub>P<sub>y</sub> with conversion and alloy mechanisms generally also go through the intercalation step, and thus their reaction process can be restricted to the intercalation stage to boost cyclic performance. For example,

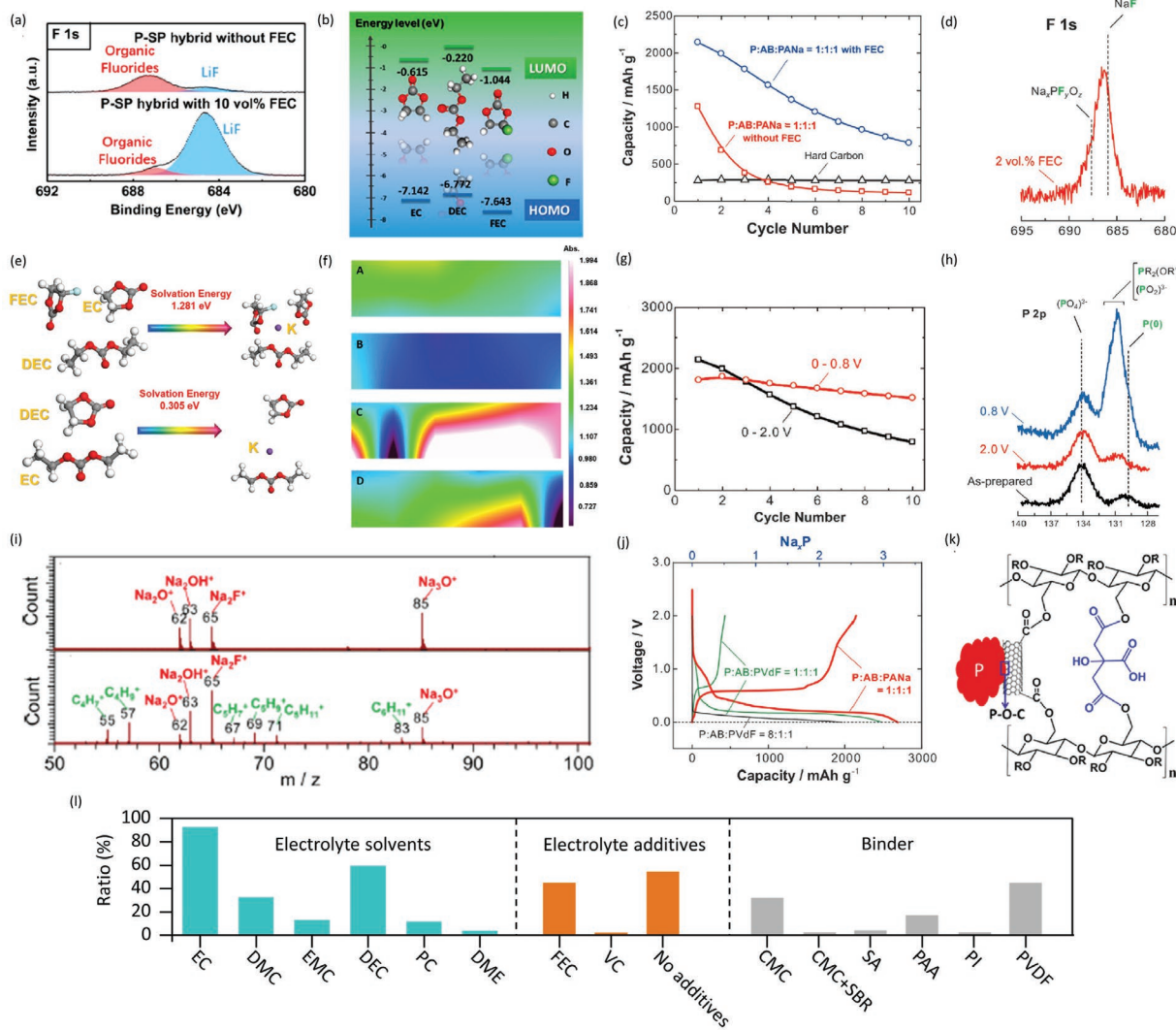


**Figure 8.** Functional electrolytes and binders exploration: a) F 1s XPS spectra for P-SP hybrid electrodes after cycling in electrolytes with and without 10 vol% FEC; b) LUMO and HOMO values of solvent molecules; c) Comparison of capacity retention with or without using FEC as the electrolyte additive; d) XPS spectra of the F 1s regions; e) Solvation energies estimated from the binding energy of the  $K^+(Y)$  clusters, where  $Y = EC+DEC$  or  $EC+DEC+FEC$ ; f) FTIR mapping of electrode surfaces after cycling in the following electrolytes. A)  $KPF_6$ -EC/DEC, B)  $KFSI$ -EC/DEC, C)  $KPF_6$ -EC/DEC with FEC, and D)  $KFSI$ -EC/DEC with FEC; g) Capacity retention of phosphorus electrodes; h) XPS spectra in the P 2p region for low-concentration P electrodes cycled with different cut-off voltages; i) TOF-SIMS positive ion spectra for BP/PANA electrodes after the second cycle; j) Galvanostatic charge/discharge curves of phosphorus electrodes with different binders; k) Interaction between P-CNT hybrid and c-NaCMC-CA binder; l) Summary of the application frequency of electrolyte solvents, additives and binders for phosphorus-based anode in literature. a,b) Reproduced with permission.<sup>[195]</sup> Copyright 2019, American Chemical Society. c,d,g,h,j) Reproduced with permission.<sup>[198]</sup> Copyright 2014, Wiley-VCH. e,f) Reproduced with permission.<sup>[121]</sup> Copyright 2018, Elsevier. i) Reproduced with permission.<sup>[196]</sup> Copyright 2016, American Chemical Society. k) Reproduced with permission.<sup>[199]</sup> Copyright 2015, American Chemical Society.

Stan et al. demonstrated that the electrochemical performance of  $Cu_3P$  depended on the depth of charge and discharge process.<sup>[30]</sup> In the case of complete discharge (0.02–2 V vs  $Li/Li^+$ ), it displayed conversion mechanism ( $Cu_3P + 3Li = Li_3P + 3Cu$ ) and poor cycling life. During partial discharge (0.5–2 V vs  $Li/Li^+$ ), it showed intercalation mechanism ( $Cu_3P + aLi = Li_aCu_3P$ ,  $a \leq 3$ ) and better cycling performance instead.

In addition, the stability of SEI can also be enhanced by optimizing charging and discharging conditions of battery. For example, Naoaki et al. reduced the upper limit voltage from 2 to 0.8 V (vs  $Na/Na^+$ ), hence its cycle performance was significantly improved due to the narrow voltage window resulting in solid SEI.<sup>[198]</sup>

## 5.5. Other Strategies

Non-active components such as conductive additives can increase conductivity, and current collectors with special treatments are able to enhance the adhesion between collector and electrode material.<sup>[200]</sup> Nitta et al. systematically explored the effects of conductive additives and current collector on the electrochemical performance of P/C, and they discovered that both CNTs and current collectors with an under layer could increase the cycling life of composites, with the specific capacity of about  $1400 \text{ mA h g}^{-1}$  after 200 cycles.<sup>[201]</sup>

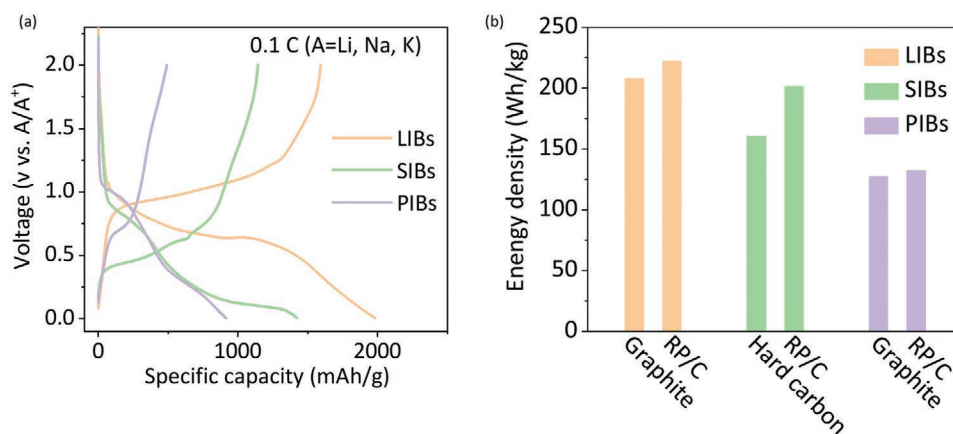


**Figure 9.** a) Charging and discharging curves in the first cycle of RP/C in AIBs; b) Energy density comparison between RP/C and commercial anode materials in AIBs (the data is based on the results in Table 1)

## 6. Application Evaluation of P Anode

The successful commercialization of silicon anode in LIBs has also attracted attention to phosphorus-based anode materials. In view of the higher specific capacity and lower potential of P anodes as compared to  $M_xP_y$  anodes, only the practical applications of P based anode are discussed herewith. Both phosphorus and silicon show huge volume expansion in the process of guest ion storage, and thus the strategies employed with them are highly similar, including the use of nano-structures, carbon coatings, alloying, core-shell structures, use of binder with high adhesion strength and conductive additives with high conductivity. However, the difference between these two anode materials with high specific capacity should also be noted. First, black phosphorus (BP) exhibits the 2D layered structure, which can be transformed into phosphorene with several atomic layer thickness by multifarious stripping methods, and it is often further compounded with graphene to improve conductivity and buffer the volume change of the composites. However, the preparation efficiency is the greatest bottleneck of the development of phosphorene materials. Second, the melting point of RP is relatively low ( $\approx 590^\circ\text{C}$ ), and thus carbon coating is difficult to achieve by gas-phase methods (such as chemical vapor deposition, CVD) or liquid-phase methods (such as wet chemical approaches, usually involving heat treatment process). Similar to the preparation of sulfur/carbon composites, RP confined in carbon materials can be synthesized by the ECC method. Nevertheless, WP produced in the synthesis process needs to be treated with toxic  $\text{CS}_2$ , which restricts its large-scale application.

For the sake of evaluate the practical application prospects of P anode in AIBs objectively, we try to synthesize RP/carbon composites (70% RP–30% Super P, RP/C) using a high energy ball milling method. The charging and discharging curves show that the first reversible specific capacity of RP/C is 1600, 1100, and 500  $\text{mA h g}^{-1}$ , and the average voltage is 0.8, 0.5, and 0.7 V (vs  $\text{A/A}^+$ ) in LIBs, SIBs and PIBs respectively (Figure 9a).

In order to estimate the energy density of phosphorus based materials in AIBs, we select cathode that have been commercialized or have the potential for commercialization and matched them with RP/C or commercial anode materials (Figure 9b and Table 1). The Energy density of batteries can be roughly calculated by the following formula:  $E_m = \frac{Q_c \times Q_a}{Q_c + Q_a} \times (U_c - U_a) \times K$  (1).

In this paper, the  $K$  value determined by the manufacturing process is set to 0.6. After calculation, it is found that the energy density of RP/C versus  $\text{LiFePO}_4$  in LIBs is only  $14.2 \text{ Wh kg}^{-1}$  higher than that of graphite versus  $\text{LiFePO}_4$ . Obviously, it is difficult for RP/C to compete with Si/carbon composites which are gradually being commercialized. As for PIBs, the energy density of RP/C versus  $\text{KFe}[\text{Fe}(\text{CN})_6]$  is only  $5.2 \text{ Wh kg}^{-1}$  higher than that of Graphite versus  $\text{KFe}[\text{Fe}(\text{CN})_6]$ .<sup>[10]</sup> Considering the low initial Coulomb efficiency (53.6%) and the great voltage polarization ( $>0.5 \text{ V vs K/K}^+$ ) of RP/C, it is apparent that there is no significant application prospect in PIBs at present. With regard to SIBs,<sup>[7]</sup> RP/C versus  $\text{Na}_3\text{V}_2(\text{PO}_4)_3$  can increase energy density by  $40.7 \text{ Wh kg}^{-1}$  compared with hard carbon versus  $\text{Na}_3\text{V}_2(\text{PO}_4)_3$ , which is the largest value in AIBs, and thus P anode is most likely to be used in SIBs in the future.

**Table 1.** Energy density comparison between RP/C and commercial anode materials in AIBs.

	Anode versus Cathode	Capacity of anode [ $\text{mA h g}^{-1}$ ]	Voltage of anode [V vs $\text{A/A}^+$ ]	Capacity of cathode [ $\text{mA h g}^{-1}$ ]	Voltage of cathode [V vs $\text{A/A}^+$ ]	Energy density [ $\text{Wh kg}^{-1}$ ]
LIBs	Graphite versus $\text{LiFePO}_4$	350	0.2	150	3.5	207.9
	RP/C versus $\text{LiFePO}_4$	1600	0.8	150	3.5	222.1
SIBs	Hard carbon versus $\text{Na}_3\text{V}_2(\text{PO}_4)_3$	250	0.1	120	3.4	160.5
	RP/C versus $\text{Na}_3\text{V}_2(\text{PO}_4)_3$	1100	0.3	120	3.4	201.2
PIBs	Graphite versus $\text{KFe}[\text{Fe}(\text{CN})_6]$	250	0.2	80	3.7	127.2
	RP/C versus $\text{KFe}[\text{Fe}(\text{CN})_6]$	500	0.5	80	3.7	132.4

It is worth noting that such the high specific capacity of RP/C is accompanied by a huge volume change. In view of the strictly limitation of volume in commercial battery systems (<20%), it is impossible to apply pure RP/C ( $>1000 \text{ mA h g}^{-1}$ ) directly as anode materials. We speculate that adding a small amount of RP/C to hard carbon to form multi-component composites will be a feasible scheme to improve the energy density of SIBs.

In addition to the capacity and voltage considerations, the low Coulomb efficiency (60–85%) of phosphorus based anode materials needs to be addressed urgently. The efficiency of anode or cathode directly determines the utilization ratio of charge carriers ( $\text{Li}^+$ ,  $\text{Na}^+$  or  $\text{K}^+$  in this paper) in full cells, which affects the energy density and cycle life of the whole battery. We believe that there are primarily four strategies that can be implemented to overcome this challenge. First, a complete and compact carbon coating layer should be formed on the surface of the phosphorus. An appropriate carbon layer can not only improve the conductivity of anodes, but also avoid the formation of massive SEI when the highly reactive phosphorus particles directly contact with electrolyte. To a certain extent, this approach can also withstand the huge volume expansion of phosphorus materials in the subsequent cycling to avoid electrode pulverization. Second, reasonable micro-nano composite structures should be designed. Although nanostructured phosphorous is usually prepared to buffer the huge volume change, the large specific surface area will reduce the first Coulombic efficiency. Micro-nano composite structures can retain the nanostructure of phosphorus, reduce the formation of SEI by the whole microstructure as well. Third, appropriate electrolyte additives need to be selected. The low

initial Coulombic efficiency of phosphorous primarily contributes to the formation of SEI by the decomposition of the electrolyte under certain electrochemical conditions. Therefore, the selection of suitable electrolyte additives, especially film-forming additives such as FEC and VC, is conducive to forming the stable SEI. Fourthly, prelithiation (presodiation, or prepotassiation) reagents can be employed. Reagents containing alkali metal ions can be added into battery system by physical, chemical or electrochemical methods to compensate the loss of active alkali metal ions in the first cycle, so as to improve the initial Coulombic efficiency and cycle life of batteries.

## 7. Conclusions and Perspectives

Phosphorus-based materials have attracted growing attention from researchers because of their high theoretical specific capacity, desirable working voltage, abundance, and low toxicity. During the charging and discharging process, RP demonstrates an alloying reaction mechanism, while BP proceeds according to first, intercalation and then alloying. In comparison,  $\text{M}_x\text{P}_y$  generally employ three mechanisms (intercalation, conversion, and alloying). However, both scientific challenges including volume expansion, unstable SEI and poor conductivity, and technical issues such as high activity in air, safety hazards, and incompatible with Cu current collector under high temperature hinder the practical application of phosphorus-based materials. The corresponding solutions are summarized in **Figure 10**.

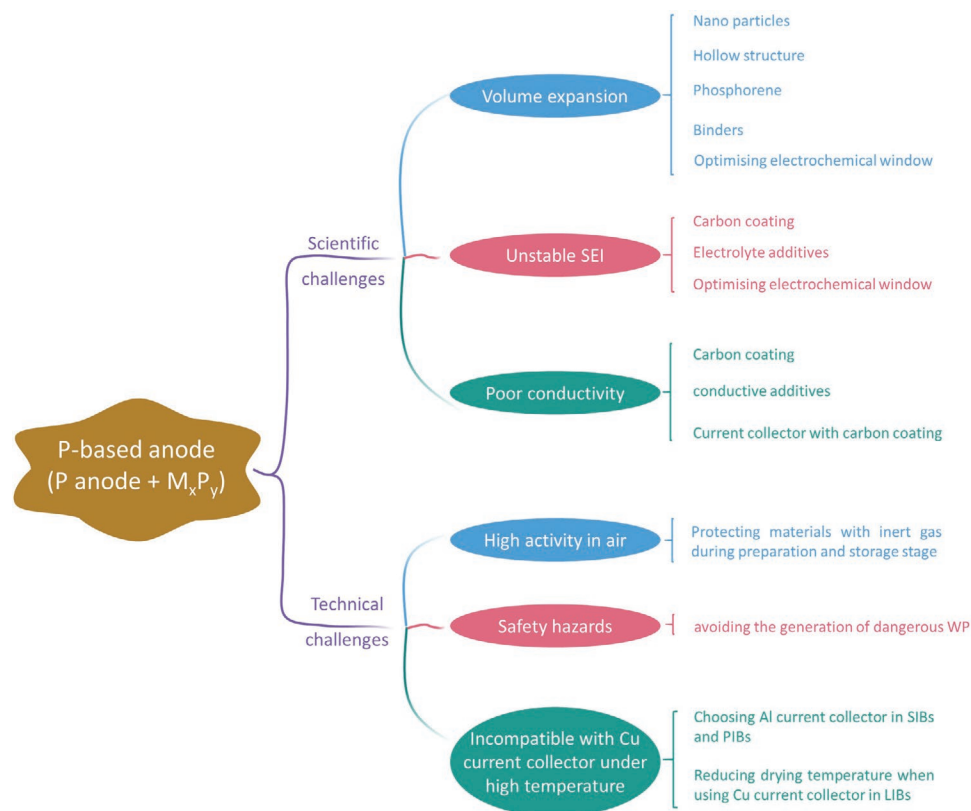


**Figure 10.** Summary of challenges and corresponding strategies for phosphorus-based materials in literature.

The future development of phosphorus-based materials may occur in the following aspects. 1) Intermediate products of phosphorus formed during the charge-discharge process are amorphous. Therefore, better characterization methods, especially in situ ones, should be used to effectively detect these products and explore the ion storage mechanism ulteriorly. 2) At present, most reported phosphorus-based materials have poor cycle performance, and only a few studies have provided detailed explanations. Hence, the failure mechanism of phosphorus-based materials in AIBs (such as volume expansion, unstable SEI, and poor conductivity) should be more deeply investigated by advanced characterization methods. 3) Many ways to synthesize phosphorus-based materials all have their own shortcomings. For example, ball milling is capable of large-scale material preparation, but the control of the product's properties such as morphology and particle size is limited. Therefore, synthesis methods that are simultaneously facile, cost effective, and highly scalable are needed, before phosphorus-based materials can be used in practical applications. 4) While many kinds of P anode and  $M_xP_y$  have been reported, there is no clear conclusion regarding the most suitable carbon materials, metal types, and their proportions for industrial applications. Better optimization of phosphorus-based materials is thus necessary. 5) Inactive materials like electrolyte additives, binders, and current collectors should be studied systematically, as they also affect the performance of the phosphorus-based materials greatly. 6) More uniform and reliable battery test conditions, such as the loading of active materials, current density, and voltage window should be put forward to facilitate objective performance comparison.

## Acknowledgements

This work was supported by the National Natural Science Foundation of China (Grant No. 51672181), the Czech Republic from ERDF "Institute of Environmental Technology – Excellent Research" (No. CZ.02.1.01/0.0/0.0/16\_019/0000853). M.H.R. thanks the Sino-German Research Institute for support (project: GZ 1400). X.Q.Y. thanks Suzhou University.

Open access funding enabled and organized by Projekt DEAL.

## Conflict of Interest

The authors declare no conflict of interest.

## Keywords

alkaline metal ion batteries, anodes, phosphorus-based materials

Received: May 31, 2020

Revised: July 20, 2020

Published online:

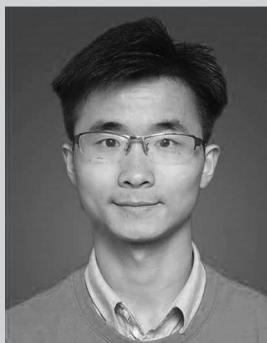
- [1] A. Kwade, W. Haselrieder, R. Leithoff, A. Modlinger, F. Dietrich, K. Droeder, *Nat. Energy* **2018**, *3*, 290.  
 [2] P. G. Bruce, S. A. Freunberger, L. J. Hardwick, J.-M. Tarascon, *Nat. Mater.* **2012**, *11*, 19.  
 [3] J.-M. Tarascon, M. Armand, *Nature* **2001**, *414*, 359.

- [4] B. Dunn, H. Kamath, J.-M. Tarascon, *Science* **2011**, *334*, 928.  
 [5] J. W. Choi, D. Aurbach, *Nat. Rev. Mater.* **2016**, *1*, 16013.  
 [6] W. Zhang, Y. Liu, Z. Guo, *Sci. Adv.* **2019**, *5*, eaav7412.  
 [7] N. Yabuuchi, K. Kubota, M. Dahbi, S. Komaba, *Chem. Rev.* **2014**, *114*, 11636.  
 [8] Z. Lin, T. Liu, X. Ai, C. Liang, *Nat. Commun.* **2018**, *9*, 5262.  
 [9] C.-X. Zu, H. Li, *Energy Environ. Sci.* **2011**, *4*, 2614.  
 [10] J.-Y. Hwang, S.-T. Myung, Y.-K. Sun, *Adv. Funct. Mater.* **2018**, *28*, 1802938.  
 [11] S. Chae, M. Ko, K. Kim, K. Ahn, J. Cho, *Joule* **2017**, *1*, 47.  
 [12] J. Ni, L. Li, J. Lu, *ACS Energy Lett.* **2018**, *3*, 1137.  
 [13] G. Chang, Y. Zhao, L. Dong, D. P. Wilkinson, L. Zhang, Q. Shao, W. Yan, X. Sun, J. Zhang, *J. Mater. Chem. A* **2020**, *8*, 4996.  
 [14] Q. Xia, W. Li, Z. Miao, S. Chou, H. Liu, *Nano Res.* **2017**, *10*, 4055.  
 [15] Y. Wu, H. B. Huang, Y. Feng, Z. S. Wu, Y. Yu, *Adv. Mater.* **2019**, *31*, 1901414.  
 [16] Y. Fu, Q. Wei, G. Zhang, S. Sun, *Adv. Energy Mater.* **2018**, *8*, 1703058.  
 [17] Y. Liu, N. Zhang, X. Liu, C. Chen, L.-Z. Fan, L. Jiao, *Energy Storage Mater.* **2017**, *9*, 170.  
 [18] X. Qin, B. Yan, J. Yu, J. Jin, Y. Tao, C. Mu, S. Wang, H. Xue, H. Pang, *Inorg. Chem. Front.* **2017**, *4*, 1424.  
 [19] L. E. Marbella, M. L. Evans, M. F. Groh, J. Nelson, K. J. Griffith, A. J. Morris, C. P. Grey, *J. Am. Chem. Soc.* **2018**, *140*, 7994.  
 [20] M. Povia, J. Sottmann, G. Portale, K. D. Knudsen, S. Margadonna, S. Sartori, *J. Phys. Chem. C* **2018**, *122*, 5917.  
 [21] J. Sun, G. Zheng, H.-W. Lee, N. Liu, H. Wang, H. Yao, W. Yang, Y. Cui, *Nano Lett.* **2014**, *14*, 4573.  
 [22] C. Peng, H. Chen, G. Zhong, W. Tang, Y. Xiang, X. Liu, J. Yang, C. Lu, Y. Yang, *Nano Energy* **2019**, *58*, 560.  
 [23] J. Sun, H.-W. Lee, M. Pasta, H. Yuan, G. Zheng, Y. Sun, Y. Li, Y. Cui, *Nat. Nanotechnol.* **2015**, *10*, 980.  
 [24] H. Jin, H. Wang, Z. Qi, T. Zhang, Y. Wan, J. Chen, C. Chuang, Y. Lu, T. Chan, H. Ju, A. Cao, W. Yan, X. Wu, H. Ji, L. Wan, *Angew. Chem., Int. Ed.* **2020**, *59*, 2318.  
 [25] D. C. S. Souza, V. Pralong, A. J. Jacobson, L. F. Nazar, *Science* **2002**, *296*, 2012.  
 [26] S. Sim, J. Cho, *J. Electrochem. Soc.* **2012**, *159*, A669.  
 [27] C.-M. Park, Y.-U. Kim, H.-J. Sohn, *Chem. Mater.* **2009**, *21*, 5566.  
 [28] S.-g. Woo, J.-H. Jung, H. Kim, M. G. Kim, C. K. Lee, H.-J. Sohn, B. W. Choe, *J. Electrochem. Soc.* **2006**, *153*, A1979.  
 [29] S.-O. Kim, A. Manthiram, *Chem. Mater.* **2016**, *28*, 5935.  
 [30] M. C. Stan, R. Klöpsch, A. Bhaskar, J. Li, S. Passerini, M. Winter, *Adv. Energy Mater.* **2013**, *3*, 231.  
 [31] F. Poli, A. Wong, J. S. Kshetrimayum, L. Monconduit, M. Letellier, *Chem. Mater.* **2016**, *28*, 1787.  
 [32] H. Pfeiffer, F. Tancret, M.-P. Bichat, L. Monconduit, F. Favier, T. Brousse, *Electrochem. Commun.* **2004**, *6*, 263.  
 [33] M. S. Chandrasekar, S. Mitra, *Electrochim. Acta* **2013**, *92*, 47.  
 [34] H. Pfeiffer, F. Tancret, T. Brousse, *Electrochim. Acta* **2005**, *50*, 4763.  
 [35] C. Villevieille, F. Robert, P. L. Taberna, L. Bazin, P. Simon, L. Monconduit, *J. Mater. Chem.* **2008**, *18*, 5956.  
 [36] S. Ni, J. Ma, X. Lv, X. Yang, L. Zhang, *J. Mater. Chem. A* **2014**, *2*, 20506.  
 [37] B. Mauvernay, M. L. Doublet, L. Monconduit, *J. Phys. Chem. Solids* **2006**, *67*, 1252.  
 [38] M.-P. Bichat, T. Politova, H. Pfeiffer, F. Tancret, L. Monconduit, J.-L. Pascal, T. Brousse, F. Favier, *J. Power Sources* **2004**, *136*, 80.  
 [39] M. P. Bichat, T. Politova, J. L. Pascal, F. Favier, L. Monconduit, *J. Electrochem. Soc.* **2004**, *151*, A2074.  
 [40] M. Fan, Y. Chen, Y. Xie, T. Yang, X. Shen, N. Xu, H. Yu, C. Yan, *Adv. Funct. Mater.* **2016**, *26*, 5019.  
 [41] A. Zhou, B. Yang, W. Wang, X. Dai, M. Zhao, J. Xue, M. Han, C. Fan, J. Li, *RSC Adv.* **2016**, *6*, 26800.  
 [42] S. O. Kim, A. Manthiram, *ACS Appl. Mater. Interfaces* **2017**, *9*, 16221.

- [43] S. Chen, F. Wu, L. Shen, Y. Huang, S. K. Sinha, V. Srot, P. A. van Aken, J. Maier, Y. Yu, *ACS Nano* **2018**, *12*, 7018.
- [44] S.-O. Kim, A. Manthiram, *Chem. Commun.* **2016**, 52, 4337.
- [45] F. Zhao, N. Han, W. Huang, J. Li, H. Ye, F. Chen, Y. Li, *J. Mater. Chem. A* **2015**, *3*, 21754.
- [46] O. Crosnier, C. Mounsey, P. S. Herle, N. Taylor, L. F. Nazar, *Chem. Mater.* **2003**, *15*, 4890.
- [47] P. Lou, Z. Cui, Z. Jia, J. Sun, Y. Tan, X. Guo, *ACS Nano* **2017**, *11*, 3705.
- [48] S. Boyanov, J. Bernardi, E. Bekaert, M. Ménétrier, M.-L. Doublet, L. Monconduit, *Chem. Mater.* **2009**, *21*, 298.
- [49] F. Gillot, S. Boyanov, L. Dupont, M.-L. Doublet, M. Morcrette, L. Monconduit, J.-M. Tarascon, *Chem. Mater.* **2005**, *17*, 6327.
- [50] K. Aso, A. Hayashi, M. Tatsumisago, *Inorg. Chem.* **2011**, *50*, 10820.
- [51] C. Wu, P. Kopold, P. A. van Aken, J. Maier, Y. Yu, *Adv. Mater.* **2017**, *29*, 4015.
- [52] Y. Feng, H. Zhang, Y. Mu, W. Li, J. Sun, K. Wu, Y. Wang, *Chem. - Eur. J.* **2015**, *21*, 9229.
- [53] Y. Lu, J. Tu, Q. Xiong, Y. Qiao, J. Zhang, C. Gu, X. Wang, S. X. Mao, *Chemistry* **2012**, *18*, 328.
- [54] S. Carenco, C. Surcin, M. Morcrette, D. Larcher, N. Mézailles, C. Boissière, C. Sanchez, *Chem. Mater.* **2012**, *24*, 688.
- [55] H. Zhang, Y. Lu, C.-D. Gu, X.-L. Wang, J.-P. Tu, *CrystEngComm* **2012**, *14*, 7942.
- [56] Y. Lu, J.-p. Tu, C.-d. Gu, X.-l. Wang, S. X. Mao, *J. Mater. Chem.* **2011**, *21*, 17988.
- [57] Y. Lu, J. P. Tu, J. Y. Xiang, X. L. Wang, J. Zhang, Y. J. Mai, S. X. Mao, *J. Phys. Chem. C* **2011**, *115*, 23760.
- [58] Y. Lu, X. Wang, Y. Mai, J. Xiang, H. Zhang, L. Li, C. Gu, J. Tu, S. X. Mao, *J. Phys. Chem. C* **2012**, *116*, 22217.
- [59] S. Shi, Z. Li, Y. Sun, B. Wang, Q. Liu, Y. Hou, S. Huang, J. Huang, Y. Zhao, *Nano Energy* **2018**, *48*, 510.
- [60] Y. Lu, J.-p. Tu, Q.-q. Xiong, Y.-q. Qiao, X.-l. Wang, C.-d. Gu, S. X. Ma, *RSC Adv.* **2012**, *2*, 3430.
- [61] Y. Lu, J.-P. Tu, Q.-Q. Xiong, J.-Y. Xiang, Y.-J. Mai, J. Zhang, Y.-Q. Qiao, X.-L. Wang, C.-D. Gu, S. X. Mao, *Adv. Funct. Mater.* **2012**, *22*, 3927.
- [62] J. Jiang, C. Wang, W. Li, Q. Yang, *J. Mater. Chem. A* **2015**, *3*, 23345.
- [63] J. Fullenwarth, A. Darwiche, A. Soares, B. Donnadieu, L. Monconduit, *J. Mater. Chem. A* **2014**, *2*, 2050.
- [64] M. i. C. López, G. F. Ortiz, J. e. L. Tirado, *J. Electrochem. Soc.* **2012**, *159*, A1253.
- [65] A. Lu, X. Zhang, Y. Chen, Q. Xie, Q. Qi, Y. Ma, D.-L. Peng, *J. Power Sources* **2015**, *295*, 329.
- [66] D. Yang, J. Zhu, X. Rui, H. Tan, R. Cai, H. E. Hoster, D. Y. Yu, H. H. Hng, Q. Yan, *ACS Appl. Mater. Interfaces* **2013**, *5*, 1093.
- [67] J. Bai, B. Xi, H. Mao, Y. Lin, X. Ma, J. Feng, S. Xiong, *Adv. Mater.* **2018**, *30*, 1802310.
- [68] K. Zhu, J. Liu, S. Li, L. Liu, Y. Yang, S. Liu, H. Wang, T. Xie, *Adv. Mater. Interfaces* **2017**, *4*, 1700377.
- [69] Y.-H. Cui, M.-Z. Xue, Z.-W. Fu, X.-L. Wang, X.-J. Liu, *J. Alloys Compd.* **2013**, *555*, 283.
- [70] W.-J. Li, Q.-R. Yang, S.-L. Chou, J.-Z. Wang, H.-K. Liu, *J. Power Sources* **2015**, *294*, 627.
- [71] V. Pralong, D. C. S. Souza, K. T. Leung, L. F. Nazar, *Electrochem. Commun.* **2002**, *4*, 516.
- [72] R. Alca'ntara, J. L. Tirado, J. C. Jumas, L. Monconduit, J. Olivier-Fourcade, *J. Power Sources* **2002**, *109*, 308.
- [73] F. Han, C. Zhang, J. Yang, G. Ma, K. He, X. Li, *J. Mater. Chem. A* **2016**, *4*, 12781.
- [74] W. J. Li, S. L. Chou, J. Z. Wang, H. K. Liu, S. X. Dou, *Chem. Commun.* **2015**, *51*, 3682.
- [75] S. Boyanov, J. Bernardi, F. Gillot, L. Dupont, M. Womes, J.-M. Tarascon, L. Monconduit, M.-L. Doublet, *Chem. Mater.* **2006**, *18*, 3531.
- [76] F. Han, C. Y. J. Tan, Z. Gao, *ChemElectroChem* **2016**, *3*, 1054.
- [77] Q.-R. Yang, W.-J. Li, S.-L. Chou, J.-Z. Wang, H.-K. Liu, *RSC Adv.* **2015**, *5*, 80536.
- [78] S. Shi, C. Sun, X. Yin, L. Shen, Q. Shi, K. Zhao, Y. Zhao, J. Zhang, *Adv. Funct. Mater.* **2020**, *30*, 1909283.
- [79] S. Shi, Z. Li, L. Shen, X. Yin, Y. Liu, G. Chang, J. Wang, S. Xu, J. Zhang, Y. Zhao, *Energy Storage Mater.* **2020**, *29*, 78.
- [80] D. C. C. Silva, O. Crosnier, G. Ouvrard, J. Greedan, A. Safa-Sefat, L. F. Nazara, *Electrochem. Solid-State Lett.* **2003**, *6*, A162.
- [81] J. W. Hall, N. Membreno, J. Wu, H. Celio, R. A. Jones, K. J. Stevenson, *J. Am. Chem. Soc.* **2012**, *134*, 5532.
- [82] C. M. S., S. Mitra, *Ionics* **2013**, *20*, 137.
- [83] Z. Huang, H. Hou, C. Wang, S. Li, Y. Zhang, X. Ji, *Chem. Mater.* **2017**, *29*, 7313.
- [84] M. G. Kim, S. Lee, J. Cho, *J. Electrochem. Soc.* **2009**, *156*, A89.
- [85] S. Kaushik, K. Matsumoto, Y. Sato, R. Hagiwara, *Electrochem. Commun.* **2019**, *102*, 46.
- [86] K.-H. Kim, C.-H. Jung, W.-S. Kim, S.-H. Hong, *J. Power Sources* **2018**, *400*, 204.
- [87] F. Gillot, M. Ménétrier, E. Bekaert, L. Dupont, M. Morcrette, L. Monconduit, J. M. Tarascon, *J. Power Sources* **2007**, *172*, 877.
- [88] Y. Kim, Y. Kim, A. Choi, S. Woo, D. Mok, N.-S. Choi, Y. S. Jung, J. H. Ryu, S. M. Oh, K. T. Lee, *Adv. Mater.* **2014**, *26*, 4139.
- [89] W. Li, S.-L. Chou, J.-Z. Wang, J. H. Kim, H.-K. Liu, S.-X. Dou, *Adv. Mater.* **2014**, *26*, 4037.
- [90] Y. Xu, B. Peng, F. M. Mulder, *Adv. Energy Mater.* **2018**, *8*, 1701847.
- [91] Q. Li, Z. Li, Z. Zhang, C. Li, J. Ma, C. Wang, X. Ge, S. Dong, L. Yin, *Adv. Energy Mater.* **2016**, *6*, 1600376.
- [92] J. Liu, P. Kopold, C. Wu, P. A. van Aken, J. Maier, Y. Yu, *Energy Environ. Sci.* **2015**, *8*, 3531.
- [93] W. Zhang, J. Mao, S. Li, Z. Chen, Z. Guo, *J. Am. Chem. Soc.* **2017**, *139*, 3316.
- [94] Y.-U. Kim, C. K. Lee, H.-J. Sohn, T. Kang, *J. Electrochem. Soc.* **2004**, *151*, A933.
- [95] B. León, J. I. Corredor, J. L. Tirado, C. Pérez-Vicentez, *J. Electrochem. Soc.* **2006**, *153*, A1829.
- [96] X. Fan, J. Mao, Y. Zhu, C. Luo, L. Suo, T. Gao, F. Han, S.-C. Liou, C. Wang, *Adv. Energy Mater.* **2015**, *5*, 1500174.
- [97] D. Lan, W. Wang, L. Shi, Y. Huang, L. Hu, Q. Li, *J. Mater. Chem. A* **2017**, *5*, 5791.
- [98] W. Li, H. Li, Z. Lu, L. Gan, L. Ke, T. Zhai, H. Zhou, *Energy Environ. Sci.* **2015**, *8*, 3629.
- [99] Y. Liu, X. Xiao, X. Fan, M. Li, Y. Zhang, W. Zhang, L. Chen, *J. Alloys Compd.* **2018**, *744*, 15.
- [100] W. Li, L. Ke, Y. Wei, S. Guo, L. Gan, H. Li, T. Zhai, H. Zhou, *J. Mater. Chem. A* **2017**, *5*, 4413.
- [101] X. Li, W. Li, P. Shen, L. Yang, Y. Li, Z. Shi, H. Zhang, *Ceram. Int.* **2019**, *45*, 15711.
- [102] W. Qi, H. Zhao, Y. Wu, H. Zeng, T. Tao, C. Chen, C. Kuang, S. Zhou, Y. Huang, *Sci. Rep.* **2017**, *7*, 43582.
- [103] D. Kim, K. Zhang, M. Cho, Y.-M. Kang, *Energy Environ. Sci.* **2019**, *12*, 1326.
- [104] M. D. Gerngross, E. Quiroga-González, J. Carstensen, H. Föll, *J. Electrochem. Soc.* **2012**, *159*, A1941.
- [105] C.-M. Park, H.-J. Sohn, *Chem. Mater.* **2008**, *20*, 6319.
- [106] J.-Y. Chen, L.-C. Chin, G.-A. Li, H.-Y. Tuan, *CrystEngComm* **2017**, *19*, 975.
- [107] H. Hwang, M. G. Kim, Y. Kim, S. W. Martin, J. Cho, *J. Mater. Chem.* **2007**, *17*, 3161.
- [108] M.-P. Bichat, J.-L. Pascal, F. Gillot, F. Favier, *J. Phys. Chem. Solids* **2006**, *67*, 1233.
- [109] M. V. V. M. Satya Kishore, U. V. Varadaraju, *J. Power Sources* **2005**, *144*, 204.
- [110] D. Duveau, S. S. Israel, J. Fullenwarth, F. Cunin, L. Monconduit, *J. Mater. Chem. A* **2016**, *4*, 3228.
- [111] Y. Lu, P. Zhou, K. Lei, Q. Zhao, Z. Tao, J. Chen, *Adv. Energy Mater.* **2017**, *7*, 1601973.

- [112] P. Poizot, S. Laruelle, S. Grugeon, L. Dupont, J.-M. Tarascon, *Nature* **2000**, 407, 496.
- [113] Y.-X. Wang, L. Huang, Y.-Q. Chang, F.-S. Ke, J.-T. Li, S.-G. Sun, *Electrochem. Commun.* **2010**, 12, 1226.
- [114] J. Y. Jang, G. Park, S.-M. Lee, N.-S. Choi, *Electrochem. Commun.* **2013**, 35, 72.
- [115] D. Lan, W. Wang, Q. Li, *Nano Energy* **2017**, 39, 506.
- [116] M. Zhang, R. Hu, J. Liu, L. Ouyang, J. Liu, L. Yang, M. Zhu, *Electrochem. Commun.* **2017**, 77, 85.
- [117] M. Walter, R. Erni, M. V. Kovalenko, *Sci. Rep.* **2015**, 5, 8418.
- [118] L. Huang, X.-M. Zheng, Y.-S. Wu, L.-J. Xue, F.-S. Ke, G.-Z. Wei, S.-G. Sun, *Electrochem. Commun.* **2009**, 11, 585.
- [119] L. Huang, Y. Yang, L.-J. Xue, H.-B. Wei, F.-S. Ke, J.-T. Li, S.-G. Sun, *Electrochem. Commun.* **2009**, 11, 6.
- [120] W. Li, X. Li, J. Liao, B. Zhao, L. Zhang, L. Huang, G. Liu, Z. Guo, M. Liu, *Energy Environ. Sci.* **2019**, 12, 2286.
- [121] W. Zhang, Z. Wu, J. Zhang, G. Liu, N.-H. Yang, R.-S. Liu, W. K. Pang, W. Li, Z. Guo, *Nano Energy* **2018**, 53, 967.
- [122] C. Lin, L. Ouyang, C. Zhou, R. Hu, L. Yang, X. Yang, H. Shao, M. Zhu, *J. Power Sources* **2019**, 443, 227276.
- [123] W. Xiao, Q. Sun, M. N. Banis, B. Wang, J. Liang, A. Lushington, R. Li, X. Li, T.-K. Sham, X. Sun, *ACS Appl. Mater. Interfaces* **2019**, 11, 30763.
- [124] C. Marino, M. El Kazzi, E. J. Berg, M. He, C. Villeveille, *Chem. Mater.* **2017**, 29, 7151.
- [125] M. C. Stan, J. v. Zamory, S. Passerini, T. Nilges, M. Winter, *J. Mater. Chem. A* **2013**, 1, 5293.
- [126] S. Haghghat-Shishavan, M. Nazarian-Samani, M. Nazarian-Samani, H.-K. Roh, K.-Y. Chung, B.-W. Cho, S. F. Kashani-Bozorg, K.-B. Kim, *J. Mater. Chem. A* **2018**, 6, 10121.
- [127] W. Li, Z. Yang, M. Li, Y. Jiang, X. Wei, X. Zhong, L. Gu, Y. Yu, *Nano Lett.* **2016**, 16, 1546.
- [128] D. B. Henge, M. Hermus, C. F. Litterscheid, N. Wagner, J. Beck, B. Albert, J. Brgoch, *Inorg. Chem.* **2015**, 54, 8761.
- [129] L.-Q. Sun, M.-J. Li, K. Sun, S.-H. Yu, R.-S. Wang, H.-M. Xie, *J. Phys. Chem. C* **2012**, 116, 14772.
- [130] B. W. Jeitschko, P. C. Donohue, *Acta Crystallogr. Sect. B: Struct. Crystallogr. Cryst. Chem.* **1972**, 28, 1893.
- [131] L. Chen, G. Zhou, Z. Liu, X. Ma, J. Chen, Z. Zhang, X. Ma, F. Li, H.-M. Cheng, W. Ren, *Adv. Mater.* **2016**, 28, 510.
- [132] Z. Huang, H. Hou, Y. Zhang, C. Wang, X. Qiu, X. Ji, *Adv. Mater.* **2017**, 29, 1702372.
- [133] V. Nicolosi, M. Chhowalla, M. G. Kanatzidis, M. S. Strano, J. N. Coleman, *Science* **2013**, 340, 1226419.
- [134] Y. Zhang, X. Rui, Y. Tang, Y. Liu, J. Wei, S. Chen, W. R. Leow, W. Li, Y. Liu, J. Deng, B. Ma, Q. Yan, X. Chen, *Adv. Energy Mater.* **2016**, 6, 1502409.
- [135] J. Zhou, X. Liu, W. Cai, Y. Zhu, J. Liang, K. Zhang, Y. Lan, Z. Jiang, G. Wang, Y. Qian, *Adv. Mater.* **2017**, 29, 1700214.
- [136] Y. Zhang, H. Wang, Z. Luo, H. T. Tan, B. Li, S. Sun, Z. Li, Y. Zong, Z. J. Xu, Y. Yang, K. A. Khor, Q. Yan, *Adv. Energy Mater.* **2016**, 6, 1600453.
- [137] R. Jain, P. Hundekar, T. Deng, X. Fan, Y. Singh, A. Yoshimura, V. Sarbada, T. Gupta, A. S. Lakhnot, S. O. Kim, C. Wang, N. Koratkar, *ACS Nano* **2019**, 13, 14094.
- [138] R. Meng, J. Huang, Y. Feng, L. Zu, C. Peng, L. Zheng, L. Zheng, Z. Chen, G. Liu, B. Chen, Y. Mi, J. Yang, *Adv. Energy Mater.* **2018**, 8, 1801514.
- [139] Q. Xie, D. Zeng, P. Gong, J. Huang, Y. Ma, L. Wang, D.-L. Peng, *Electrochim. Acta* **2017**, 232, 465.
- [140] J. Y. Xiang, X. L. Xiang, J. Zhong, D. Zhang, J. P. Tu, *J. Power Sources* **2011**, 196, 379.
- [141] X. Ge, Z. Li, L. Yin, *Nano Energy* **2017**, 32, 117.
- [142] Z. Li, L. Zhang, X. Ge, C. Li, S. Dong, C. Wang, L. Yin, *Nano Energy* **2017**, 32, 494.
- [143] Z. Liu, S. Yang, B. Sun, P. Yang, J. Zheng, X. Li, *Angew. Chem., Int. Ed.* **2020**, 59, 1975.
- [144] J. Xu, I.-Y. Jeon, J. Ma, Y. Dou, S.-J. Kim, J.-M. Seo, H. Liu, S. Dou, J.-B. Baek, L. Dai, *Nano Res.* **2017**, 10, 1268.
- [145] Y. Kim, Y. Park, A. Choi, N.-S. Choi, J. Kim, J. Lee, J. H. Ryu, S. M. Oh, K. T. Lee, *Adv. Mater.* **2013**, 25, 3045.
- [146] C.-M. Park, H.-J. Sohn, *Adv. Mater.* **2007**, 19, 2465.
- [147] J. Qian, X. Wu, Y. Cao, X. Ai, H. Yang, *Angew. Chem., Int. Ed.* **2013**, 52, 4633.
- [148] L. Wang, X. He, J. Li, W. Sun, J. Gao, J. Guo, C. Jiang, *Angew. Chem.* **2012**, 1, 124.
- [149] J. Qian, D. Qiao, X. Ai, Y. Cao, H. Yang, *Chem. Commun.* **2012**, 48, 8931.
- [150] B. Peng, Y. Xu, K. Liu, X. Wang, F. M. Mulder, *ChemElectroChem* **2017**, 4, 2140.
- [151] Y. Wang, L. Tian, Z. Yao, F. Li, S. Li, S. Ye, *Electrochim. Acta* **2015**, 163, 71.
- [152] I. Sultana, M. M. Rahman, T. Ramireddy, Y. Chen, A. M. Glushenkov, *J. Mater. Chem. A* **2017**, 5, 23506.
- [153] Z. Xu, Y. Zeng, L. Wang, N. Li, C. Chen, C. Li, J. Li, H. Lv, L. Kuang, X. Tian, *J. Power Sources* **2017**, 356, 18.
- [154] X. Li, G. Chen, Z. Le, X. Li, P. Nie, X. Liu, P. Xu, H. B. Wu, Z. Liu, Y. Lu, *Nano Energy* **2019**, 59, 464.
- [155] Y. Zhu, Y. Wen, X. Fan, T. Gao, F. Han, C. Luo, C. Liou, C. Wang, *ACS Nano* **2015**, 9, 3254.
- [156] Y. Zhang, L. Wang, H. Xu, J. Cao, D. Chen, W. Han, *Adv. Funct. Mater.* **2020**, 30, 1909372.
- [157] W. C. Chang, J. H. Wu, K. T. Chen, H. Y. Tuan, *Adv. Sci.* **2019**, 6, 1801354.
- [158] T. Yuan, J. Ruan, C. Peng, H. Sun, Y. Pang, J. Yang, Z.-F. Ma, S. Zheng, *Energy Storage Mater.* **2018**, 13, 267.
- [159] Z. Yu, J. Song, D. Wang, D. Wang, *Nano Energy* **2017**, 40, 550.
- [160] W.-J. Li, S.-L. Chou, J.-Z. Wang, H.-K. Liu, S.-X. Dou, *Nano Lett.* **2013**, 13, 5480.
- [161] G.-L. Xu, Z. Chen, G.-M. Zhong, Y. Liu, Y. Yang, T. Ma, Y. Ren, X. Zuo, X.-H. Wu, X. Zhang, K. Amine, *Nano Lett.* **2016**, 16, 3955.
- [162] L. Sun, Y. Zhang, D. Zhang, J. Liu, Y. Zhang, *Nano Res.* **2018**, 11, 2733.
- [163] W. Li, Z. Yang, Y. Jiang, Z. Yu, L. Gu, Y. Yu, *Carbon* **2014**, 78, 455.
- [164] X. Sun, W. Li, X. Zhong, Y. Yu, *Energy Storage Mater.* **2017**, 9, 112.
- [165] Y. Wu, S. Hu, R. Xu, J. Wang, Z. Peng, Q. Zhang, Y. Yu, *Nano Lett.* **2019**, 19, 1351.
- [166] Y. Liu, Q. Liu, A. Zhang, J. Cai, X. Cao, Z. Li, P. D. Asimow, C. Zhou, *ACS Nano* **2018**, 12, 8323.
- [167] Y. Liu, A. Zhang, C. Shen, Q. Liu, X. Cao, Y. Ma, L. Chen, C. Lau, T.-C. Chen, F. Wei, C. Zhou, *ACS Nano* **2017**, 11, 5530.
- [168] Z. Yu, J. Song, M. L. Gordin, R. Yi, D. Tang, D. Wang, *Adv. Sci.* **2015**, 2, 1400020.
- [169] H. Gao, T. Zhou, Y. Zheng, Y. Liu, J. Chen, H. Liu, Z. Guo, *Adv. Energy Mater.* **2016**, 6, 1601037.
- [170] Z. Yue, T. Gupta, F. Wang, C. Li, R. Kumar, Z. Yang, N. Koratkar, *Carbon* **2018**, 127, 588.
- [171] J. Zhou, Z. Jiang, S. Niu, S. Zhu, J. Zhou, Y. Zhu, J. Liang, D. Han, K. Xu, L. Zhu, X. Liu, G. Wang, Y. Qian, *Chem* **2018**, 4, 372.
- [172] L. Pei, Q. Zhao, C. Chen, J. Liang, J. Chen, *ChemElectroChem* **2015**, 2, 1652.
- [173] X. Ma, L. Chen, X. Ren, G. Hou, L. Chen, L. Zhang, B. Liu, Q. Ai, L. Zhang, P. Si, J. Lou, J. Feng, L. Ci, *J. Mater. Chem. A* **2018**, 6, 1574.
- [174] G.-H. Lee, M. R. Jo, K. Zhang, Y.-M. Kang, *J. Mater. Chem. A* **2017**, 5, 3683.
- [175] Q. Tan, W. Zhao, K. Han, P. Li, W. A. Wang, D. He, Z. Liu, Q. Yu, M. Qin, X. Qu, *J. Mater. Chem. A* **2019**, 7, 15673.
- [176] J. Song, Z. Yu, M. L. Gordin, S. Hu, R. Yi, D. Tang, T. Walter, M. Regula, D. Choi, X. Li, A. Manivannan, D. Wang, *Nano Lett.* **2014**, 14, 6329.

- [177] C. Zhang, X. Wang, Q. Liang, X. Liu, Q. Weng, J. Liu, Y. Yang, Z. Dai, K. Ding, Y. Bando, J. Tang, D. Golberg, *Nano Lett.* **2016**, *16*, 2054.
- [178] L. Sun, Y. Zhang, D. Zhang, Y. Zhang, *Nanoscale* **2017**, *9*, 18552.
- [179] G. Zeng, X. Hu, B. Zhou, J. Chen, C. Cao, Z. Wen, *Nanoscale* **2017**, *9*, 14722.
- [180] S. H. Weihan Li, X. Luo, Z. Li, X. Sun, M. Li, F. Liu, Y. Yu, *Adv. Mater.* **2017**, *29*, 1605820.
- [181] S. Yao, J. Cui, J. Huang, J.-Q. Huang, W. G. Chong, L. Qin, Y.-W. Mai, J.-K. Kim, *Adv. Energy Mater.* **2017**, *17*, 1702267.
- [182] C. Marino, A. Debenedetti, B. Fraisse, F. Favier, L. Monconduit, *Electrochem. Commun.* **2011**, *13*, 346.
- [183] C. Marino, L. Boulet, P. Gaveau, B. Fraisse, L. Monconduit, *J. Mater. Chem.* **2012**, *22*, 22713.
- [184] D. Liu, X. Huang, D. Qu, D. Zheng, G. Wang, J. Harris, J. Si, T. Ding, J. Chen, D. Qu, *Nano Energy* **2018**, *52*, 1.
- [185] Y. Wu, Z. Liu, X. Zhong, X. Cheng, Z. Fan, Y. Yu, *Small* **2018**, *14*, 1703472.
- [186] P. Xiong, P. Bai, S. Tu, M. Cheng, J. Zhang, J. Sun, Y. Xu, *Small* **2018**, *8*, 1802410.
- [187] B. Liu, Q. Zhang, L. Li, Z. Jin, C. Wang, L. Zhang, Z.-M. Su, *ACS Nano* **2019**, *13*, 13513.
- [188] W.-J. Li, S.-L. Chou, J.-Z. Wang, H.-K. Liu, S.-X. Dou, *J. Mater. Chem. A* **2016**, *4*, 505.
- [189] Y. Sun, L. Wang, Y. Li, Y. Li, H. R. Lee, A. Pei, X. He, Y. Cui, *Joule* **2019**, *3*, 1080.
- [190] C. Ferrara, E. Vigo, B. Albin, P. Galinetto, C. Milanese, C. Tealdi, E. Quartarone, S. Passerini, P. Mustarelli, *ACS Appl. Energy Mater.* **2019**, *2*, 2794.
- [191] K. Zhang, M. Park, J. Zhang, G.-H. Lee, J. Shin, Y.-M. Kang, *Nano Res.* **2017**, *10*, 4337.
- [192] J. Yang, Y. Zhang, C. Sun, H. Liu, L. Li, W. Si, W. Huang, Q. Yan, X. Dong, *Nano Res.* **2016**, *9*, 612.
- [193] W. Li, J. Yu, J. Wen, J. Liao, Z. Ye, B. Zhao, X. Li, H. Zhang, M. Liu, Z. Guo, *J. Mater. Chem. A* **2019**, *7*, 16785.
- [194] K. Xu, *Chem. Rev.* **2004**, *104*, 4303.
- [195] W. Lei, Y. Liu, X. Jiao, C. Zhang, S. Xiong, B. Li, J. Song, *ACS Appl. Energy Mater.* **2019**, *2*, 2699.
- [196] M. Dahbi, N. Yabuuchi, M. Fukunishi, K. Kubota, K. Chihara, K. Tokiwa, X.-f. Yu, H. Ushiyama, K. Yamashita, J.-Y. Son, Y.-T. Cui, H. Oji, S. Komaba, *Chem. Mater.* **2016**, *28*, 1625.
- [197] S. Choi, T.-w. Kwon, A. Coskun, J. W. Choi, *Science* **2017**, *357*, 279.
- [198] N. Yabuuchi, Y. Mitsuura, T. Satoru, J.-Y. Son, Y.-T. Cui, H. Oji, S. Komaba, *ChemElectroChem* **2014**, *1*, 580.
- [199] J. Song, Z. Yu, M. L. Gordin, X. Li, H. Peng, D. Wang, *ACS Nano* **2015**, *9*, 11933.
- [200] R. Wang, H. Mo, S. Li, Y. Gong, B. He, H. Wang, *Sci. Rep.* **2019**, *9*, 675.
- [201] N. Nitta, D. Lei, H. R. Jung, D. Gordon, E. Zhao, G. Gresham, J. Cai, I. Lutzenov, G. Yushin, *ACS Appl. Mater. Interfaces* **2016**, *8*, 25991.
- [202] J. Qian, Y. Xiong, Y. Cao, X. Ai, H. Yang, *Nano Lett.* **2014**, *14*, 1865.
- [203] D. Zhao, B. Li, J. Zhang, X. Li, D. Xiao, C. Fu, L. Zhang, Z. Li, J. Li, D. Cao, C. Niu, *Nano Lett.* **2017**, *17*, 3376.



**Junhua Zhou** is presently a doctoral student in the Soochow Institute for Energy and Materials InnovationS (SIEMIS), Soochow University, China. He received M. Eng. from the Institute of Functional Nano and Soft Materials (FUNSOM), Soochow University, China in 2018. His research mainly focuses on the alloy-based materials in alkali metal ion batteries.



**Ruizhi Yang** is a full professor at College of Energy, Soochow University, China. She received her B.S. degree in Material Science from Hunan University and Ph.D. degree in Condensed Matter Physics from the Institute of Physics, Chinese Academy of Sciences (2005). She worked as a post-doctoral fellow at Dalhousie University, Canada, from 2005 to 2008. She then moved to USA, working as a research associate at Stanford University from 2008 to 2011, prior to joining Soochow University. Her research interests cover electrocatalysis, metal-air batteries and solid state lithium batteries.



**Mark H. Rummeli** heads the electron microscopy labs at the Soochow Institute for Energy and Materials InnovationS (SIEMIS), Soochow University. He also oversees the gas sensor laboratory at Polish Academy of Sciences, Zabzre. His research focuses on the growth mechanisms of nanostructures and their functionalization and their application in electronic devices, biomedicine, and energy storage.